We are IntechOpen, the world's leading publisher of Open Access books Built by scientists, for scientists

6,900
Open access books available

185,000
International authors and editors

200M
Downloads

Our authors are among the

154
Countries delivered to

TOP 1%
most cited scientists

12.2%
Contributors from top 500 universities



WEB OF SCIENCE™

Selection of our books indexed in the Book Citation Index in Web of Science™ Core Collection (BKCI)

Interested in publishing with us?
Contact book.department@intechopen.com

Numbers displayed above are based on latest data collected.
For more information visit www.intechopen.com



11

Design and Characterization of Metamaterials for Optical and Radio Communications

André de Lustrac, Shah Nawaz Burokur, Boubacar Kanté, Alexandre Sellier and Dylan Germain
Institut d'Electronique Fondamentale, Univ. Paris-Sud, CNRS UMR 8622, Orsay, France

1. Introduction

Metamaterials have attracted considerable interests (Shelby, 2001, Yen, 2004, Smith, 2004, Linden, 2004, Zhang, 2004) because of their unusual electromagnetic properties (Veselago, 1968) and because of their potential applications such as invisibility cloaks (Leonhardt, 2006, Pendry, 2006, Schurig, 2006, Cai, 2007, Gaillot, 2008, Kante, 2008), the so-called perfect lenses (Pendry, 2000) and gradient index (GRIN) lenses. For example, perfect lenses require the use of Left-Handed (LH) metamaterials (Smith, 2000) having a negative refractive index, which can be produced by a simultaneously negative electric permittivity ε and magnetic permeability μ. Invisibility cloaks require adjustable positive permeability and permittivity from near zero values to several tenths. Traditionally, these properties are achieved by the use of a combination of split-ring resonators (Pendry, 1999) and metallic wires (Pendry, 1996), with periods much smaller than the wavelength of the electromagnetic wave, such that the medium can be considered homogeneous. Lately, pairs of finite-length wires (cut wires pairs) (Shalaev, 2005) have been proposed not only to replace the conventional split-ring resonators (SRRs) to produce a negative magnetic permeability under normal to plane incidence, but also lead to a negative refractive index n in the optical regime. However in a recent review paper (Shalaev, 2007), Shalaev stated that it is very difficult to achieve a negative refractive index with exclusively wire pairs and that the negative index value observed in the ref. (Shalaev, 2005), was accomplished in part because of the significant contribution from the imaginary part of the permeability. Nevertheless, the negative index from only cut wire and plate pairs has never been verified elsewhere (Dolling, 2005). Instead, continuous wires have been combined to the cut wire pairs to produce simultaneously a negative permittivity to lead to a negative index in the microwave domain (Zhou, 2006a). Zhou *et al*. also theoretically proposed a left-handed material using only cut wire pairs by increasing the equivalent capacitance between two consecutive short wire pairs so as to adjust the electric resonance frequency (Zhou, 2006b) This increase of capacitance can only be obtained by strongly reducing the spacing between two consecutive wires, which is quite difficult to achieve at high frequencies. These cited results concern mainly the microwave domain. In the optical regime, infrared and visible domains, the main problem concern the design and the characterization of metamaterials made of unit cells

with nanometric dimensions. At this scale, the control and the engineering of the electromagnetic properties of metamaterials are closely linked to the easiness of the fabrication. This easiness is more and more important with the simplicity of the geometrical shapes of the unit cell of the metamaterials. We show that we can change the conventional shape of the split ring resonator of J. Pendry to simple coupled nanowires, keeping the same electromagnetic properties (Linden, 2004, Enkrich, 2005, Kante, 2008a, Burokur, 2009a).

In the first part of this chapter we investigate numerically and experimentally the electromagnetic properties of cut wire pairs metamaterials where the symmetry between the wires on opposite faces is voluntarily broken along the **E**-field direction (Sellier, 2009, Kante, 2009a, Burokur, 2009a). It is reported that in this case the electric resonance of the cut wire pairs can occur at lower frequencies than the magnetic resonance, which is in contrast with the symmetrical configuration. This lower electrical resonance frequency allows realizing a common frequency region where the permeability and the permittivity are simultaneously negative. This claim is verified numerically and experimentally in the microwave domain and indications on designing negative refractive index from structures composed of only cut wire pairs are given.

Then, we investigate numerically and experimentally the reflection and transmission spectra for an obliquely incident plane wave on the asymmetric structure. It is reported that a diffraction threshold appears in E-plane (plane containing vectors E and k), that is the (-1,0) mode starts to propagate (Burokur, 2009b). Besides, resonances in E-plane shift in frequency with increasing oblique incidence. However in H-plane (plane containing vectors H and k), the structure is diffractionless and independent of the incidence and therefore the negative index is maintained in a wide angular range. These statements are verified numerically and experimentally in the microwave domain.

On the other hand, we show that it is possible to engineer the resonances of metamaterial in the infrared domain (Kante, 2008b, Kante, 2009b). We present an experimental and numerical analysis of the infrared response of metamaterials made of split ring resonators (SRR) and continuous nanowires deposited on silicon when the geometry of the SRRs is gradually altered. The impact of the geometric transformation of the SRRs on the spectra of the composite metamaterial is measured in the 1.5-15 μm wavelength range for the two field polarizations under normal to plane propagation. We show experimentally and numerically that tuning the SRRs towards elementary cut wires translates in a predictable manner the wavelength response of the artificial material. We also analyze coupling effects between the SRRs and the continuous nanowires for different spacing between them. The results of our study are expected to provide useful guidelines for the design of optical devices using metamaterials on silicon.

2. Cut wire pairs metamaterials with broken symmetry at microwave frequencies

2.1 Plasmon hybrization

In this chapter, we show that negative dielectric permittivity and negative magnetic permeability can be simultaneously achieved by appropriately controlling the coupling strength between paired cut-wires of adjacent layers. The coupling strength is itself

controlled by adjusting either the spacing or the alignment of paired cut-wires. Using an asymmetric alignment, an inverted hybridization scheme, where the asymmetric mode is at a higher frequency than the symmetric mode, is predicted and thus more favorable for obtaining negative refraction. The first experimental demonstration of a negative refraction metamaterial exclusively based on paired cut-wires in the microwave range is reported.

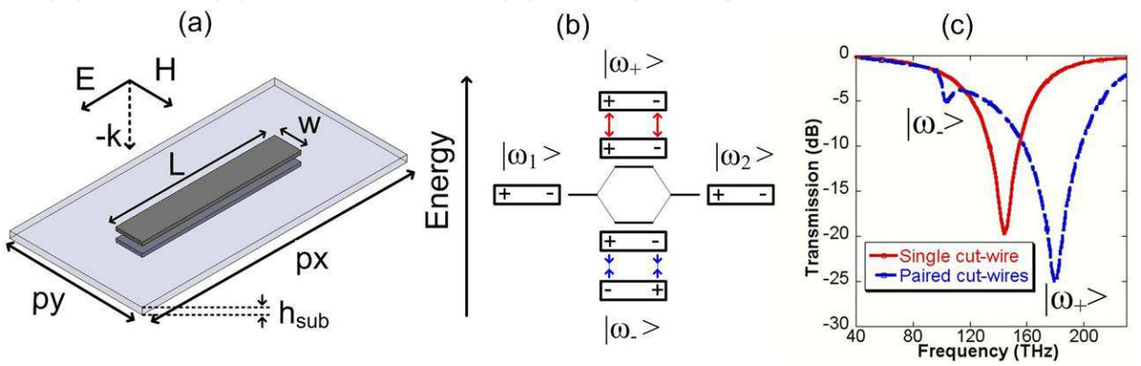


Fig. 1. (a) Schematic of the symmetric cut-wire pair. (b) Hybridization scheme of the two coupled dipoles. (c) Transmission spectra calculated at normal incidence for a periodic array of cut-wires (red) and of paired cut-wires (blue), respectively (px= 1.2 μm; py= 200 nm; w= 30 nm; L= 600 nm; hsub= 100 nm). The 30 nm thick gold cut-wires are described using a Drude model whose parameters can be found in [Kante, 2008a]. The dielectric spacer (SiO2) permittivity is ε_{sub}=2.25.

The plasmon hybridization scheme was introduced by Prodan et al. [Prodan, 2003] who gave an intuitive electromagnetic analogue of molecular orbital theory. Such a scheme has largely been used by the metamaterial community especially for simplifying metamaterial designs at optical wavelengths [Shalaev, 2005, Liu, 2008]. The coupling of two electric dipoles facing each other has thus been exploited to mimic magnetic atoms and alter the effective magnetic permeability of metamaterials in the optical range. While a magnetic activity was indeed obtained from metamaterials comprised of metallic dipoles [Shalaev, 2005, Liu, 2008], negative refraction was reported only in the pioneering demonstration by Shalaev et al. [Shalaev, 2005] who used a periodic array of cut-wire pairs. In order to unambiguously achieve negative refraction, the magnetic activity must actually occur within a frequency band in which the electric permittivity is negative. For this purpose, one solution consists of associating magnetic "atoms" (coupled metallic dipoles) to a broadband "electric plasma" (continuous wires) in the same structure. Many authors have used this solution either in the microwave [Zhou, 2006, Guven, 2006] or in the optical regime [Liu, 2008], thereby contributing to the development of the so-called fishnet structure. We propose another solution based on the control of the coupling between metallic dipoles in such a way that the symmetric and anti-symmetric bands have a sufficient overlap. The coupling strength is varied either by changing the distance between coupled dipoles or by breaking the symmetry of the structure.

Fig. 1(a) shows the rectangular unit cell of the studied 2D structure in the case where the coupled metallic dipoles (cut-wires) are vertically aligned. This structure is henceforth referred to as the symmetric cut-wire structure to distinguish it from the asymmetric

structure discussed later (see fig. 2). Both structures consist of 2D periodic arrays of metallic cut-wires separated by a dielectric spacer [Shalaev, 2005]. The electromagnetic wave should propagate normally to the layers with the electric field parallel to the longest side of dipolar elements. The structure can be described in terms of effective parameters as long as the cut-wire width w and spacer thickness hsub are much smaller than the wavelength [Shalaev, 2005]. Two series of calculations were carried out using a finite element simulation package (HFSS from Ansys), one for symmetric structures and the other for asymmetric structures. The effective parameters were obtained from the calculated transmission and reflection coefficients [Gundogdu, 2008].

The first series of calculations were performed to compare the electromagnetic response of a symmetric cut-wire bi-layer (blue curve in Fig. 1(c)) to that of a cut-wire monolayer (red curve in Fig. 1(c)). As it is evident in the figure, only one resonance is observed for the single-face cut-wire structure in the frequency range of interest. This resonance corresponds to the fundamental cut-wire dipolar mode, which in the optical regime can also be interpreted in terms of a localized plasmon resonance [Smith, 2002]. Collective electronic excitations, also called surface plasmons, are indeed the main mechanism at short wavelengths. For the double-face cut-wire structure, the coupling between paired cut-wires lifts the degeneracy of the single cut-wire mode, which hybridizes into two plasmon modes. One mode is symmetric and corresponds to in-phase current oscillations, while the other is anti-symmetric and corresponds to out-of-phase current oscillations. For a symmetric cut-wire pair with a vertical alignment of the two cut-wires, the anti-symmetric mode is the low-energy (-frequency) mode since attractive forces are present in the system. Conversely, repellent forces are produced in the case of the symmetric mode that is therefore the high-frequency mode. The stronger the coupling (the smaller the spacing between the dipoles), the larger the frequency difference between the two modes. The evolution of the transmission spectra with the thickness of the dielectric spacer (or substrate) h_{sub} is illustrated in Fig. 3(a) in the case of a structure designed to operate in the microwave regime. Similar results were obtained for the structure in Fig. 1(c).

A second series of calculations was performed to analyze the influence of a vertical misalignment of metallic dipoles at a fixed spacer (or substrate) thickness. For this purpose, the cut-wire layers were shifted from each other in the horizontal XY plane (Fig. 2(a)) thus breaking the symmetry of the cut-wire structure. The relative displacements dx and dy in the X and Y directions respectively were used as parameters. In the example in the microwave regime, the substrate thickness was chosen to be equal to that of commercially available epoxy dielectric boards (1.2 mm). For this thickness and a vertical alignment of paired cut-wires (dx = dy = 0), the calculated transmission spectrum in Fig. 3(a) revealed a pronounced frequency separation between the symmetric (electric) and anti-symmetric (magnetic) modes. Figs. 3(b) and 3(c) show the evolution of the transmission spectrum for non-zero values of the longitudinal (dx) and lateral (dy) displacements, respectively. Quite surprisingly, as previously reported by A. Christ et al. [Christ, 2007] for the control of Fano resonances in a plasmonic lattice of continuous wires, symmetry breaking can invert the hybridization scheme due to modified Coulomb interactions (Fig. 2(b)) resulting in the symmetric resonance occurring at a lower frequency than the anti-symmetric one. The Coulomb forces in our system result from the interaction of charges located at the cut-wire ends. When the longitudinal shift (dx) is progressively increased, the signs of the charges in

close interaction change. As a result the repulsive force becomes attractive and vice versa. Correspondingly, the symmetric mode becomes the low-energy mode while the asymmetric mode is shifted to higher frequencies. It is evident that this inversion process is impossible in the case of a lateral dy displacement of the dipoles (Fig. 3(c)).

Controlling the coupling between metallic dipoles thus allows the two plasmon resonances to be engineered. When the magnetic and electric modes are very close together, the bands of negative permeability and negative permittivity overlap, and a negative refraction material is obtained. More generally, the design of true negative index metamaterials can be achieved by appropriate design of the three degrees of freedom h_{sub}, dx and dy.

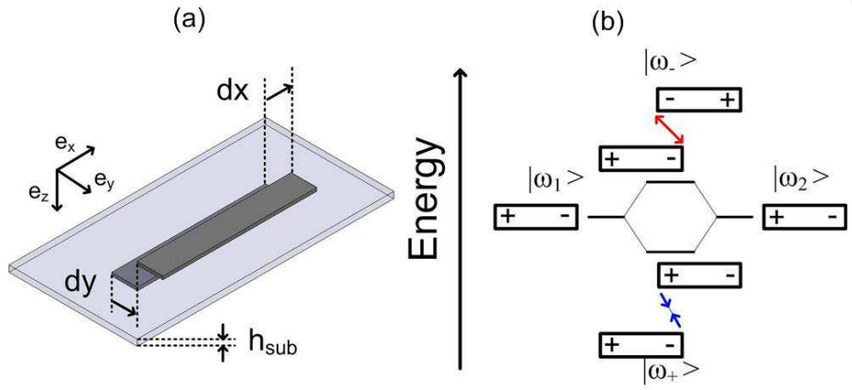


Fig. 2. (a) Asymmetric cut-wire pair with the three degrees of freedom for the control of the coupling strength: hsub, dx and dy. (b) Inverted hybridization scheme.

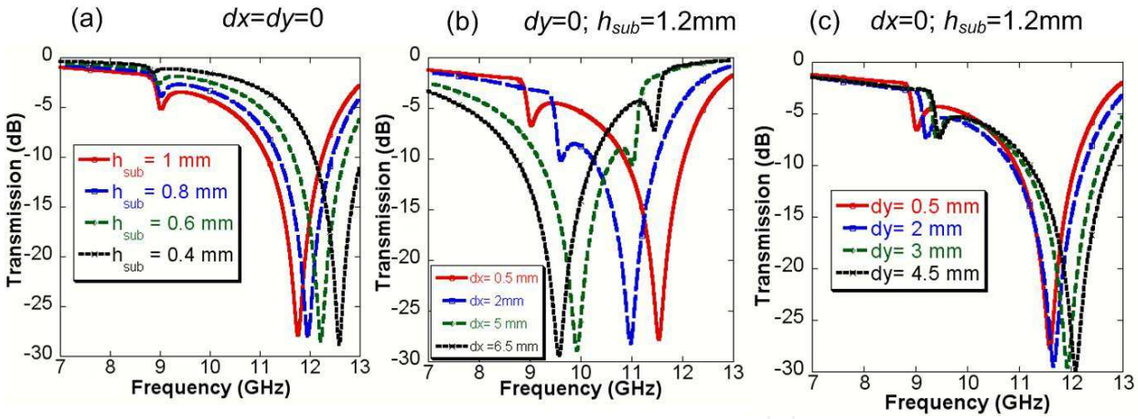


Fig. 3. Influence of the coupling strength on the transmission spectra of a bi-layer structure (px = 19 mm; py = 9.5 mm; w = 0.3 mm; L = 9.5 mm; h_{sub} = 1.2 mm). The substrate permittivity is ε_{sub} = 3.9. (a) variation of the dielectric spacer (or substrate) thickness h_{sub}; (b) variation of the longitudinal shift dx; (c) variation of the lateral shift dy.

2.2 Monolayer double-face structure

In this part, we present a systematic study of the cut wires structure presented in Fig. 4, derived from the previous structures, under normal-to-plane incidence in the microwave domain. Numerical simulations performed using the FEM based software HFSS are run to

show and understand the electromagnetic behavior of the design. A single layer of the metamaterial is characterized by reflection and transmission measurements. The retrieved parameters show simultaneous resonances in the permittivity and permeability responses leading to a negative index of refraction.

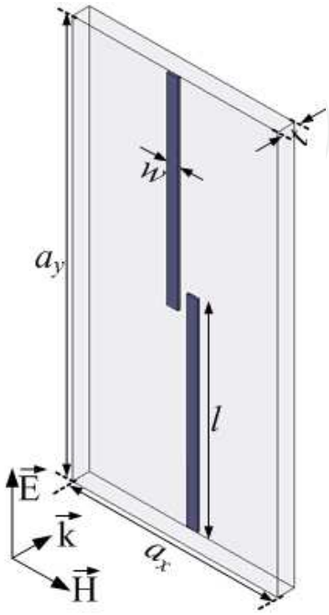


Fig. 4. Unit cell of: cut wires structure under normal-to-plane propagation (ax = 9.5 mm, ay = 19 mm, w = 0.3 mm, l = 9.5 mm). The inserts show the direction and the polarization of the wave.

The cut wires metamaterial illustrated by its unit cell in Fig. 4 is employed to operate in the microwave regime. It consists of a double-face structure composed of periodic cut wires of finite length. The structure is printed on both faces of an epoxy dielectric board of thickness t = 1.2 mm and of relative permittivity ε_r = 3.9. For the different samples reported here, the width of the cut wires denoted by w is 0.3 mm. The length of the cut wires is l = 9.5 mm and the unit cell size in the x and y direction is respectively ax = 9.5 mm and ay = 19 mm. These dimensions have been optimized to operate around 10 GHz and remain the same throughout the section.

The reflection and transmission spectra of the metamaterial are calculated using HFSS by applying the necessary periodic boundary conditions on the unit cell. Several samples of the structure consisting of 10 × 5 cells on a 120 mm × 120 mm epoxy surface are fabricated using conventional commercial chemical etching technique. Measurements are done in an anechoic chamber using an Agilent 8722ES network analyzer and two X-band horn antennas. In the transmission measurements, the plane waves are incident normal to the prototype surface and a calibration to the transmission in free space (the metamaterial sample is removed) between the two horn antennas is done. The reflection measurements are done by placing the emitting and receiving horn antennas on the same side of the prototype and inclined with an angle of about 5° with respect to the normal on the prototype surface. The calibration for the reflection is done using a sheet of copper as reflecting mirror.

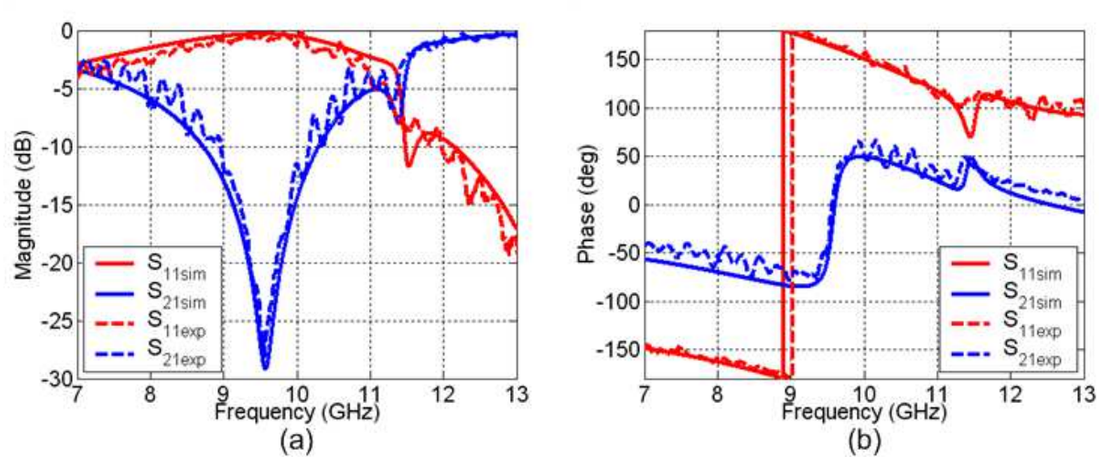
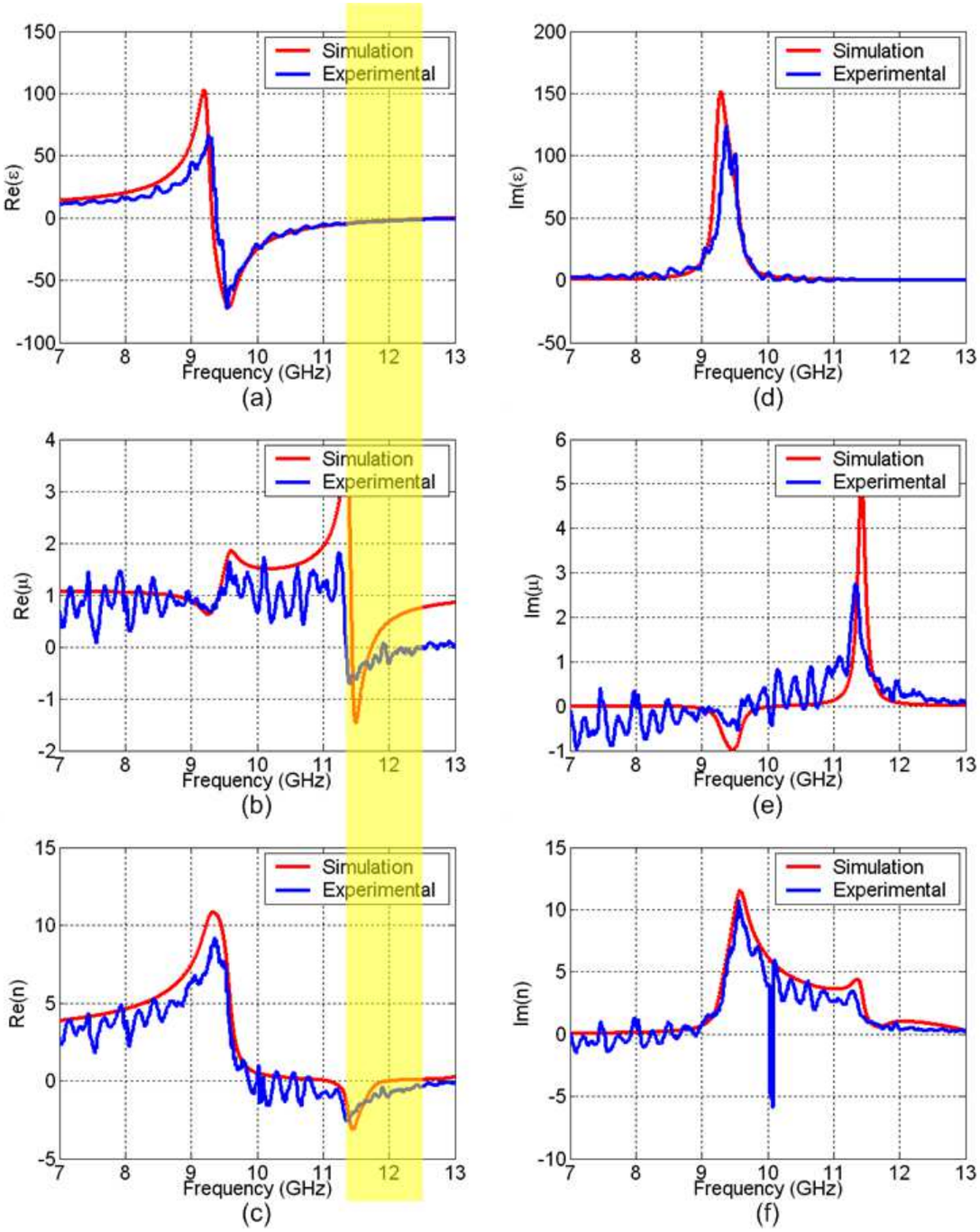


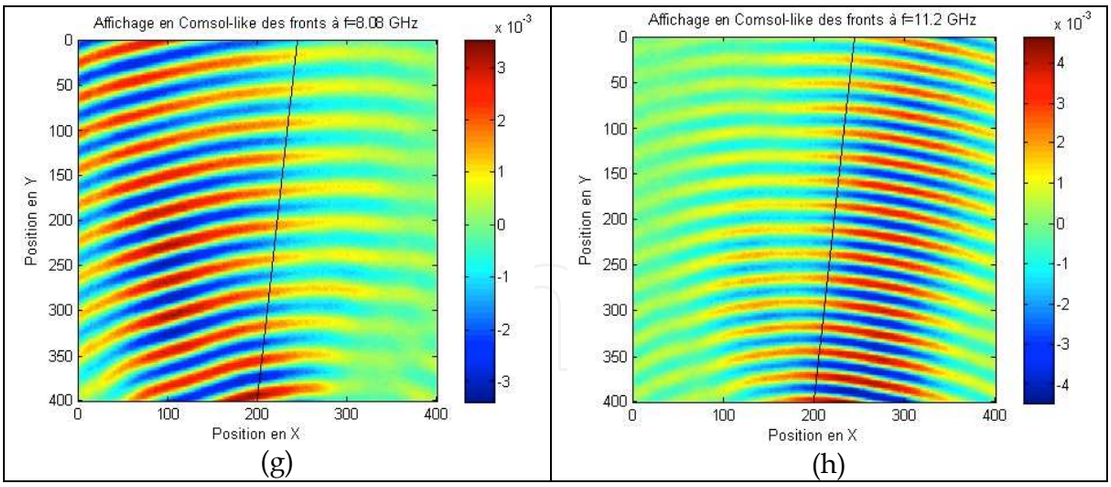
Fig. 5. Calculated and measured reflection (S11) and transmission (S21) responses of the metamaterial for a single layer: (a) magnitude, and (b) phase.

Figure 5 shows the calculated (continuous lines) and measured (dashed lines) S-parameters of the metamaterial for a monolayer configuration. There is a very good qualitative agreement between simulations and measurements. The calculated and measured magnitudes of S21 presented in Fig. 5(a) show clearly two resonance dips, the first one at 9.58 GHz and a second one at 11.39 GHz. We can note in Fig. 5(b) that a change in sign occurs for the transmission phase at the first resonance dip. At the second resonance dip, a peak and a dip is respectively observed in the transmission and reflection phase.

Using the retrieval procedure described in [Nicholson, 1970], based on the inversion of the reflection and transmission coefficients, the effective parameters of the double-face metamaterial structure are extracted. The metamaterial has a period very small compared to the wavelength λ (less than λ/20) in the propagation direction. The propagation of the electromagnetic wave travelling along this direction is dominated by this deep sub-wavelength period and not by the in-plane period ax or ay. There is only a single propagating mode in the negative-index frequency region, justifying the description of the cut wires metamaterial with an effective index [Valentine, 2008].

The extracted permittivity ε, permeability μ and refractive index n are shown in the various parts of Fig. 6. Two extraction procedures have been performed: the first one uses the calculated S-parameters and the second one is based on the measured S-parameters. As illustrated by the extracted parameters from the calculated and measured S-parameters, the cut wires structure shows firstly an electric resonance at the first resonance dip observed at 9.58 GHz in Fig. 6. This electric resonance exhibits values going negative for the real part of the permittivity in the vicinity of the resonance. Secondly a magnetic resonance with negative values appears at the right hand side of the second resonance dip at 11.5 GHz. Around the same frequency, the real part of the permittivity is still negative. The extracted real part of the refractive index is therefore negative around 11.5 GHz which is the frequency of the LH peak. However, we can also notice that the zero value for the ε response is very close to 13 GHz where a full transmission band is observed in Fig. 6(a). This frequency constitutes the frequency of the RH transmission peak. We can therefore deduce that this RH transmission peak is due to an impedance matching between the structure and vacuum.


Simulation
Experimental
Re(ε)
Frequency (GHz)
(a)
Im(ε)
(d)
Re(μ)
(b)
Im(μ)
(e)
Re(n)
(c)
Im(n)
(f)



(g) (h)

Fig. 6. Extracted electromagnetic properties of the cut wires metamaterial using the simulated and experimental data of Fig. 4: (a)-(c) real parts, and (d)-(f) imaginary parts of the permittivity ε, of the permeability μ and the refraction index n. The shaded yellow area delineates the frequency region where the measured real parts of ε and μ are simultaneously negative. Measurement of the wave propagation trough a prism of 6.3°: (g) E field cartography at 8.08GHz: the optical index is positive, around 5.6 (h) E field cartography at 11.2GHz: the optical index is negative, around -2.3.

Since the real part of n (n′) is given by n′ = ε′z′ - ε′′z′′ from n = εz and z = √(μ/ε), the imaginary parts of the permittivity (ε′′) and the permeability (μ′′) also accounts for n′. Therefore, a negative real part of n can be accomplished without having ε′ and μ′ simultaneously negative. This can happen only if ε′′ and μ′′ are sufficiently large compared to ε′ and μ′. A wider negative n′ frequency band is observed due to the dispersion of the fabricated prototype. The shaded yellow area in Fig. 6 highlights the frequency region where the measured real parts of the permittivity (ε′) and the permeability (μ′) are simultaneously negative to emphasize the desired measured negative values of n′. Concerning the imaginary parts, a very good qualitative agreement is observed between calculations and experiments. We shall note that the imaginary part of n (n′′) is very low in the negative n′ frequency region. Figures 6(g) and 6(h) show the measurements of the near electric field through a prism with an angle of 6.3°. Figure 6(g) shows the E field cartography at 8.08 GHz: the optical index is positive and found to be around 5.6. Figure 6(h) shows the E field cartography at 11.2 GHz: the optical index is negative and calculated to be around -2.3. These values agree very well with the extracted values of the optical index calculated from the measurements of the reflexion and transmission coefficients of the figure 6(c) using the retrieval procedure described in [Nicholson, 1970].

2.3 Stacking of layers

Stacking multiple layers of LH materials may be useful in many practical applications such as subwavelength imaging [Wang, 2007, Ziolkowski, 2003] and directive antennas [Burokur, 2005, Shelby, 2001]. It is obvious that the effective properties obtained from the inversion method on a monolayer give a good idea about the effective properties of the metamaterial. However, other effect such as inter-layer coupling must be taken into account because it

affects the material properties of the structure. Therefore, two, three and four layers of the designed bi-layered metamaterial are stacked with a 1 mm air spacing between each layer as presented in Fig. 7(a). Numerical simulations are run to show the expected performances of a bulk metamaterial composed of multiple layers. The transmission spectra for the different number of layers are presented in Fig. 7(b).

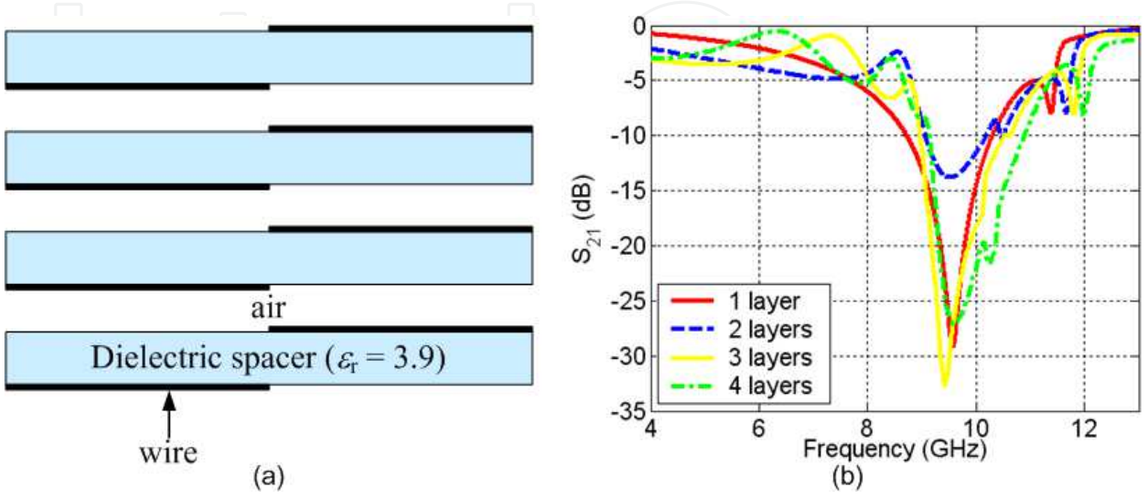


Fig. 7. (a) A bulk metamaterial composed of four layers interleaved with 1 mm air spacing, and (b) transmission spectra for different number of layers.

From the spectra of Fig 7(b), we can note that the frequency of the first transmission dip remains constant with an increasing number of layers while the second dip shifts slightly towards higher frequencies. However, peaks and valleys appear at lower frequencies suggesting a coupling mechanism between consecutive layers. The number of these peaks and valleys increases with an increasing number of layers as shown in Fig. 7(b). The transmission spectra together with the corresponding reflection spectra are used for the extraction of the material properties presented in Fig. 8. It should be noted that the first transmission dip in the single layer case corresponds to an electric resonance where ε' exhibits negative values. However, other $\varepsilon' < 0$ frequency bands can be observed in Fig. 8(a) for the multiple layers cases due to the valleys noted in the transmission spectra. And, since the magnitude of the transmission dips decreases with the number of layers, the magnitude of ε' also decreases as shown in Fig. 8(a). At higher frequencies near 12 GHz, a magnetic resonance is also observed for multiple layers as for the single layer case. However the magnitude tends to decrease while the number of layers increases (Fig. 8(b)). For more than two layers, μ' exhibits only positive values at the resonance near 12 GHz. Besides, another magnetic resonance with $\mu' < 0$ can be observed at lower frequencies with simultaneously $\varepsilon' < 0$ when more than one layer is used. So even if the $\mu' < 0$ frequency band disappears at the second transmission dip due to the $\mu' > 0$, a negative index band is observed at lower frequencies as shown in Fig. 8(c). This negative refractive index results from the coupling mechanism created when several layers of the double-face structure are stacked. The negative index frequency band widens when the number of layers increases.

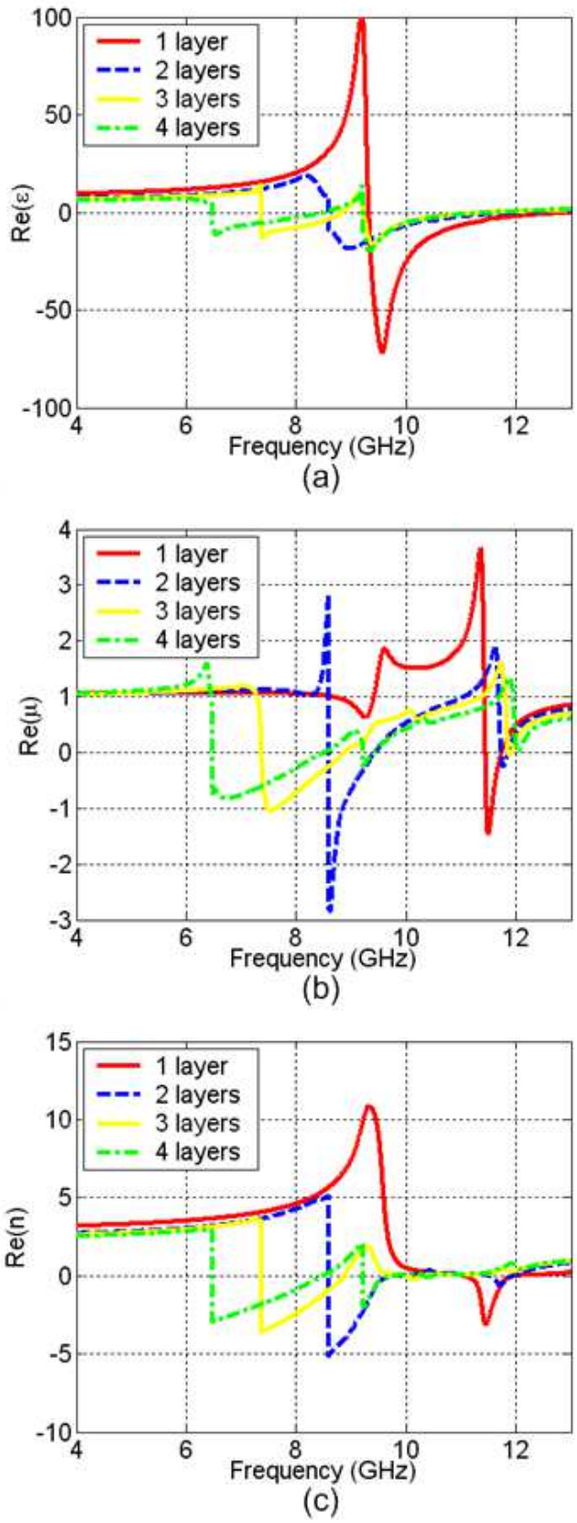


Fig. 8. Extracted material properties for different number of layers. (a) Re(ε), (b) Re(μ), and (c) Re(n).

2.4 Incidence dependence of the negative index

Finally, we investigate numerically and experimentally the reflection and transmission spectra for an obliquely incident plane wave on the asymmetric structure. Three different angles, namely 15°, 30° and 45° in both H- and E-planes of the square lattice are studied in simulations and experiments. Measured reflection and transmission coefficients are compared to simulated ones in Fig. 9 for the H-plane. There is qualitative agreement between simulations and measurements. Calculated and measured magnitudes of S_{21} show clearly two resonance dips, an electric one at 9.5 GHz and a magnetic one at 11.5 GHz. These two resonances are found to be independent of the incidence angle in the H-plane as shown in Figs. 9(a)-(c).

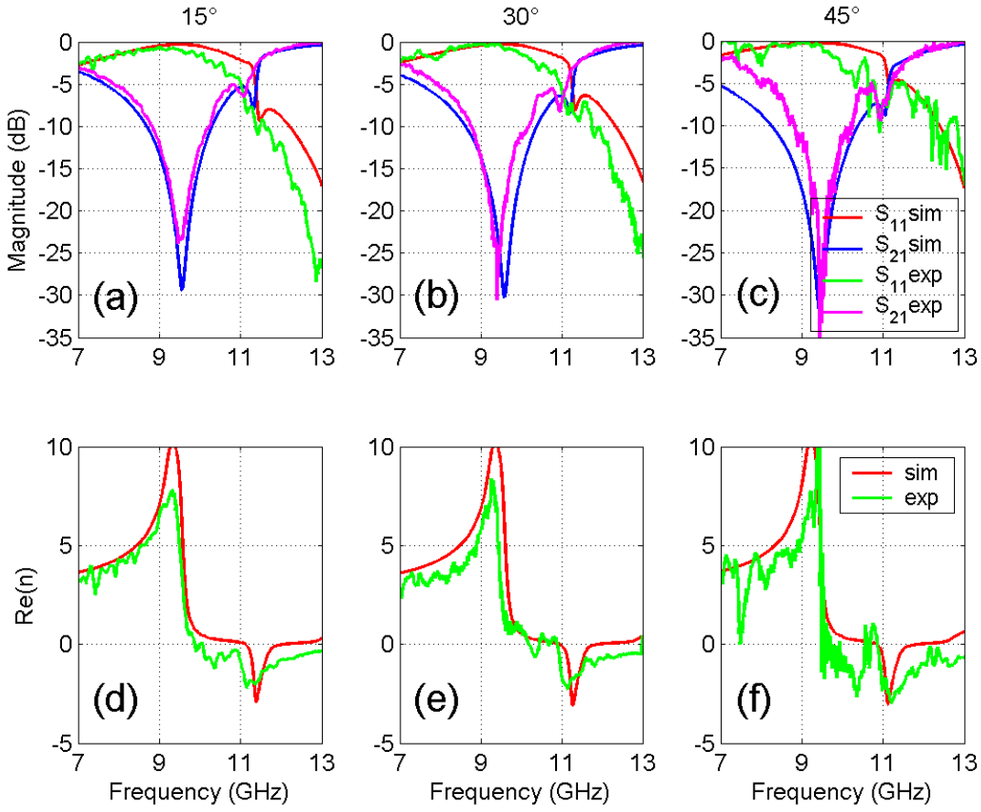


Fig. 9. Oblique incidence (15°, 30° and 45°) in H-plane. (a)-(c) Computed and measured reflection and transmission coefficients. (d)-(f) Real part of effective index n.

To retrieve effective parameters at oblique incidence, the retrieval procedure in [Smith, 2002] has to be modified and anisotropy has to be addressed [Burokur, 2009b]. Indeed cut wire pairs represent a biaxial anisotropic media whose principal axis are along x, y and z. Consequently 2x2 transfer matrices used in normal incidence are no longer sufficient and the full 4x4 transfer matrix accounting for coupling of s- and p-waves should be considered [Yeh, 1998]. However, since the electric field in our case is always along y independently of θ, cross-polarization terms do not arise and therefore we only use one 2x2 matrix for s-waves. In this case the effective index is given by

$$\frac{\varepsilon_y \mu_x \mu_z}{\mu_z \cos^2\theta + \mu_x \sin^2\theta} \tag{1}$$

Figures 9(d)-(f) show that n responses remain mostly unchanged compared to the 0° case studied in [Burokur, 2009, Sellier, 2009].

Measured reflection and transmission coefficients are compared to simulated ones in Fig. 10 for the E-plane. Apart from one sharp feature on each spectrum, simulations and measurements agree qualitatively. This peak which is much sharper than either the anti-symmetric or the symmetric resonance, shifts with incidence angles from 12.47 GHz at 15° to 10.5 GHz at 30° and 9.22 GHz at 45°. It is the manifestation on the specular order (0,0) of a diffraction threshold, namely that of the (0,-1) diffracted order. At these frequencies the (0,-1) diffracted order transits from evanescent to propagating, appearing at grazing incidence. Diffraction thresholds frequencies are calculated in two ways, with HFSS and using (2) from grating theory taking into account the fact that there is no wave vector component along x in E-plane.

$$k_\perp = \pm\sqrt{\frac{\omega^2}{c^2}\varepsilon_r - k_{//}^2} = \pm\sqrt{\frac{\omega^2}{c^2}\varepsilon_r - \left(m\frac{2\pi}{a_x}\right)^2 - \left(\frac{\omega}{c}\sin\theta + n\frac{2\pi}{a_y}\right)^2} \quad m,n \in Z \tag{2}$$

Due to respective values of ax = 9.5 mm and ay = 19 mm, it can be seen that the (0,-1) order is the first diffracted order to become propagating. Results for diffraction thresholds frequencies are summarized in Table I. By comparison, in the H-plane even at an angle of 45° the (0,-1) diffracted order is above 18 GHz. To overcome the appearance of a diffraction threshold, a triangular lattice as shown in the inset of Fig. 10(d) is proposed to replace the square one used in the figure 10(a-c). In the triangular lattice, every other cell along x is laterally displaced by 4.75 mm along y. In this lattice, diffraction threshold frequencies are given by (3):

$$k_\perp = \pm\sqrt{\frac{\omega^2}{c^2}\varepsilon_r - k_{//}^2} = \pm\sqrt{\frac{\omega^2}{c^2}\varepsilon_r - \left((2m-n)\frac{2\pi}{a_x}\right)^2 - \left(\frac{\omega}{c}\sin\theta + n\frac{2\pi}{a_y}\right)^2} \quad m,n \in Z \tag{3}$$

Computed reflection and transmission spectra presented in Figs. 10(d)-(f) confirm the rejection of the diffraction threshold above 13 GHz. Besides, a shift in frequency can be noted for both anti-symmetric and symmetric resonances. This shift is seen to be much stronger than for any resonances in the H-plane and the detuning of both electric and magnetic resonances with respect to the incidence angle θ leads to a loss of the frequency overlap, hence the negative index, above 20°. As it can be noted particularly for θ = 15°, the magnetic resonance shifts towards lower frequencies for the triangular lattice (10.43 GHz) compared to the square one (11.02 GHz). This is most probably due to extra capacitive coupling between y-displaced wires on same face of the dielectric board.

In summary, we presented the dependence of resonances and retrieved effective index on the incident angle in recently proposed asymmetric cut wire pairs. No change has been observed for oblique incidence in the H-plane. However for the E-plane, a diffraction threshold appears for the square lattice rendering the introduction of effective parameters

meaningless. A triangular lattice has therefore been proposed to avoid having the diffraction threshold below the electric and magnetic resonances. A detuning of both resonances has been observed leading to a lack of resonance frequencies overlap above 20°.

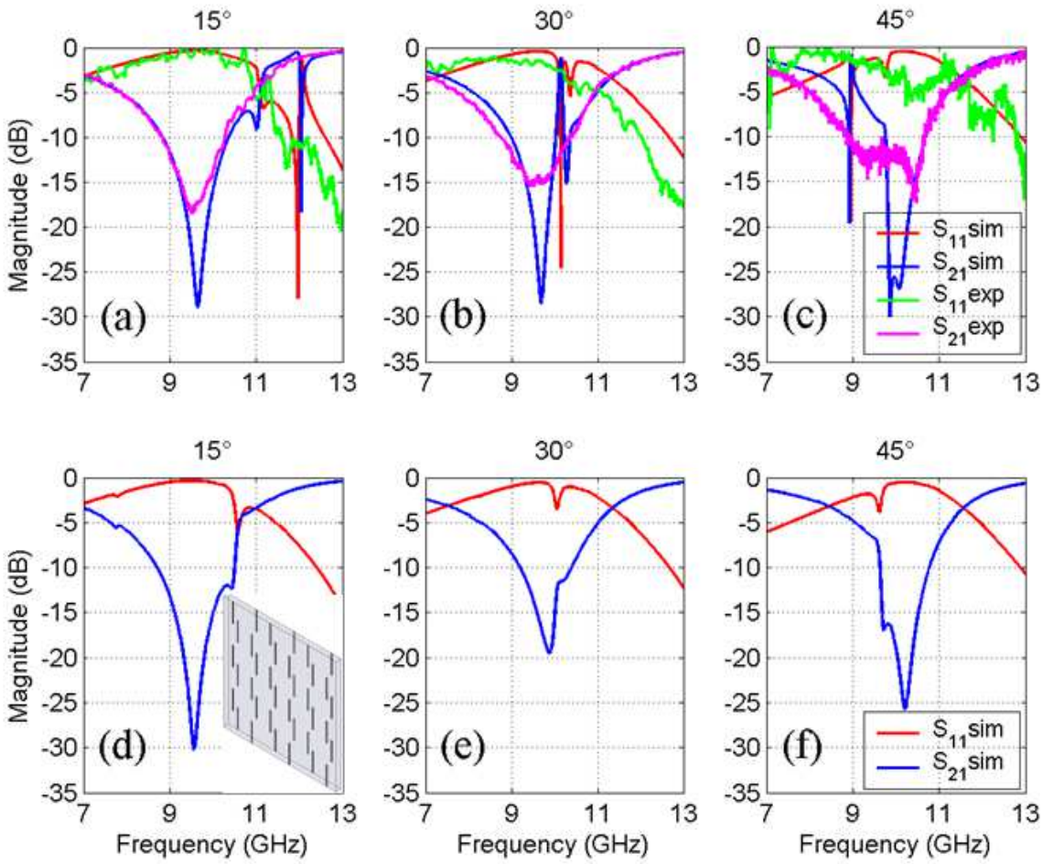


Fig. 10. Oblique incidence (15°, 30° and 45°) in E-plane. (a)-(c) Computed and measured reflection and transmission coefficients for the square lattice. (d)-(f) Computed and measured reflection and transmission coefficients for the triangular lattice.

	HFSS (square lattice) Mode (0,-1)	Grating (square lattice) Mode (0,-1)	HFSS (triangular lattice) Mode (0,-1)	Grating (triangular lattice) Mode (0,-1)
$\theta = 0°$	15.78	15.79	22.31	22.33
$\theta = 15°$	12.58	12.54	19.15	19.15
$\theta = 30°$	10.54	10.53	17.31	17.32
$\theta = 45°$	9.24	9.25	16.35	16.35

Table 1. Computed numerical and analytical diffraction threshold frequencies (GHz)

3. Infrared metamaterials and plasmons hybridization

3.1 Engineering resonances in infrared metamaterials

Recently, a theoretical study showed that optical resonances in both SRR arrays and cut wire arrays could be interpreted in terms of plasmon resonances [Rockstuhl, 2006]. A gradual shift in the SRR resonance frequencies was predicted when reducing the length of SRR legs to the point where each SRR was transformed into a single wire piece. The magnetic and electric properties of these modified versions of SRRs were theoretically investigated in [Zhou, 2007]. Following these theoretical studies, we present here an experimental and numerical analysis of the infrared response of metamaterials made of continuous nanowires and split ring resonators where the geometry is gradually altered. The metamaterial structure is fabricated on low-doped silicon. The impact of the geometric transformation of the SRRs on the spectra of the composite metamaterial is measured in the 20-400 THz frequency range (i.e., in the 1.5 - 15 μm wavelength range) for the two field polarizations under normal to plane propagation. Coupling effects between the SRRs and the continuous nanowires are analyzed for different spacings between them. The results of our study are expected to provide useful guidelines for the design and engineering of negative index metamaterials on silicon.

3.1.1 Design, fabrication, characterization and modeling of metamaterial structures

Four structures consisting of a two-dimensional periodic array of gold nanowires and gold SRRs were fabricated on a 280μm thick silicon substrate (Fig. 11). The fabrication steps included e-beam lithography, high vacuum electron beam evaporation of 5 nm thick titanium and 40 nm thick gold films, and a lift-off process. It is worthwhile noticing that all structures were fabricated in the same run, thereby allowing a meaningful comparison of their optical characteristics. As seen in Fig. 11, the four structures only differ in the shape of SRRs, which are gradually transformed into simple cut wires from structure 1 to structure 4. In the intermediate cases of structures 2 and 3, SRRs appear to be U-shaped with smaller legs than in the standard case of structure 1. Except for this resonator shape, all the other geometrical parameters of the four structures are identical. In each case, the lattice period is ~ 600nm, the width of all wires (continuous and discontinuous) is ~ 50nm, and the continuous wires are parallel to the SRR bases with a separation of 115 ± 20 nm between each continuous wire and the closest SRR base. The SRR gap width in structure 1 is ~100 nm while the length of the two SRR legs is ~ 280nm. This length is reduced to ~190 and 110 nm in structures 2 and 3, respectively. The scanning electron microscope (SEM) images reported in Fig. 11 (middle row) illustrate the excellent regularity of the four fabricated structures.

The transmission and reflection spectra of the fabricated structures were measured under normal-to-plane incidence with a FTIR (Fourier Transformed InfraRed spectrometer) BioRad FTS 60 equipped with a Cassegrain microscope. The FTIR beam was polarized using a KRS5 polarizer adapted to the wavelength region from ~ 1.5 to 15μm (i.e. to frequencies varying from 20 to 200 THz). A diaphragm was used in such a way as to produce a light spot smaller than 100 × 100 μm2 onto the sample (i.e. smaller than the surface of each periodic structure). Measurements were performed for two field polarizations of the incident beam, the parallel polarization with the illuminating electric field parallel to both the continuous wires and the SRR gaps and the perpendicular polarization with the electric field perpendicular to the

continuous wires and SRR gaps. The measured transmission spectra were normalized versus the transmission of an unprocessed part of the silicon substrate. The measured reflection spectra were normalized versus the reflection of a 40 nm thick gold film deposited on silicon.

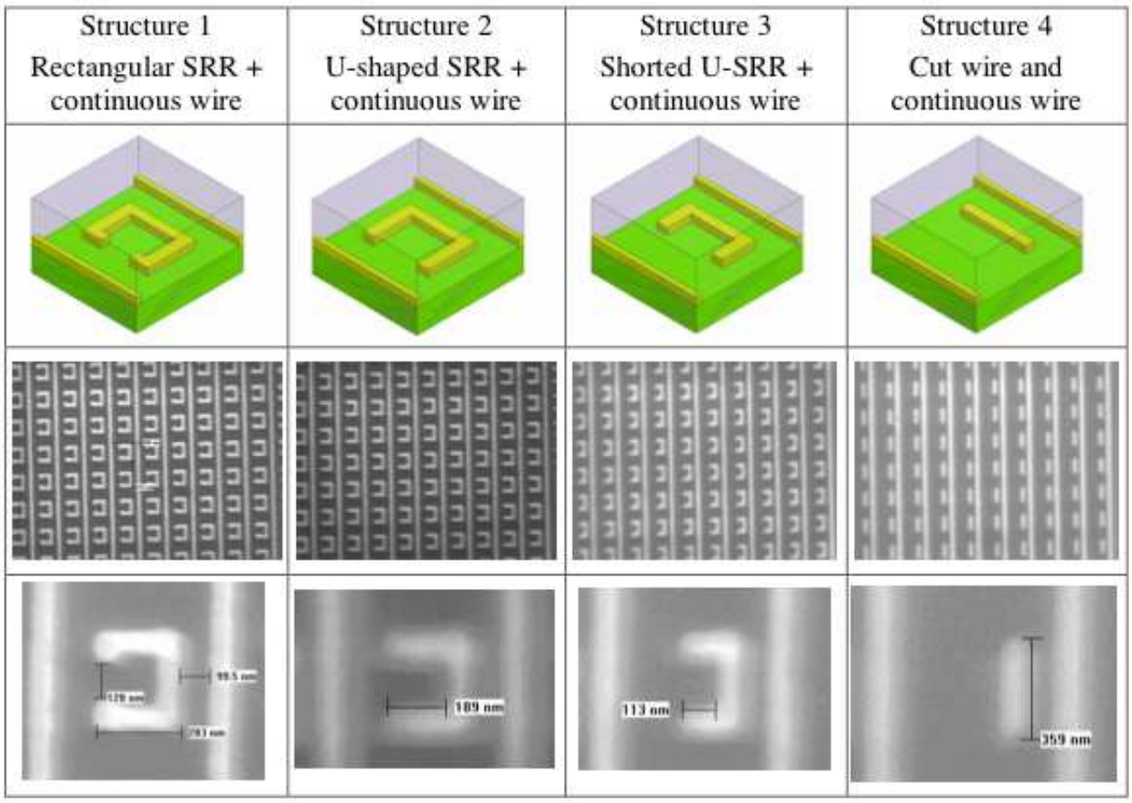


Fig. 11. Schematic representations (top) and scanning electron microscope images (middle and bottom) of the four metamaterial structures fabricated on silicon. The top and bottom pictures show the elementary unit cell of each structure. From left to right, the length of SRR legs is reduced to the point where the SRR is transformed into a single wire piece. The middle pictures show the regularity achieved in the fabrication of the periodic arrays of nanowires and split ring resonators

Numerical simulations of the spectral responses of the four structures were performed with a finite element software (HFSS, 2006). Periodic boundary conditions were applied to the lateral sides of the elementary lattice cell (Fig. 11). The silicon substrate was assumed to be lossless with a constant permittivity equal to 11.9. A Drude model was used to simulate the permittivity and loss tangent of the gold wires:

$$\varepsilon(\omega) = 1 - \frac{\omega_p^2}{\omega(\omega + i\omega_c)} \tag{4}$$

where ω_p and ω_c are the plasma and collision frequency of the gold film, respectively. The values of ω_p and ω_c chosen in the simulations were: ω_p =1.367 x 10^{16}s^{-1} (f_p =2176 THz) and ω_c

= 6.478 x 10^{13} s^{-1} (f_c =10.3 THz). Actually, the collision frequency can be considered to a certain extent as a fit parameter. An increase of the collision frequency results in higher absorption losses of the structures, while it does not change the spectral positions of resonances. The value reported above for ω_c is 2.6 times larger than in bulk gold. This increase is supposed to account for additional scattering experienced by electrons at the metal surfaces.

3.1.2 Results of measurements and simulations

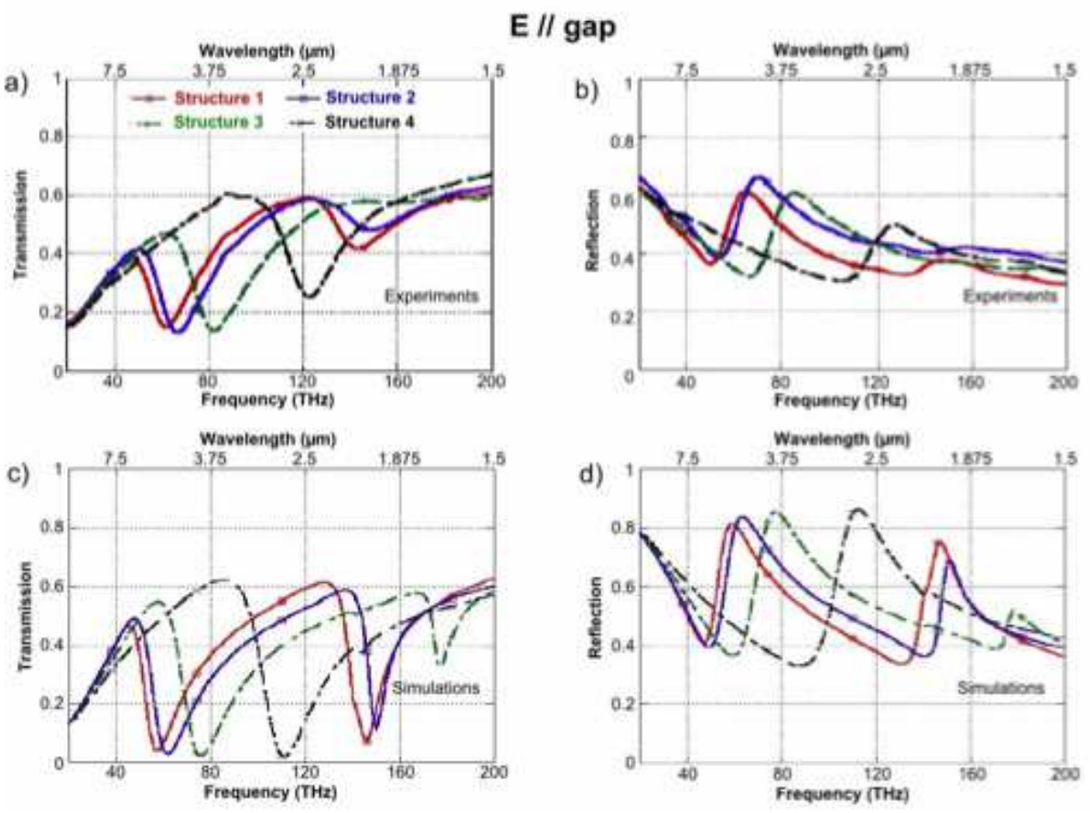
The results of our measurements and simulations are shown in Fig. 12 for the four structures. Results for the parallel polarization are gathered in the series of figures from (a) to (d). Those for the perpendicular polarization are gathered in the series of figures from (e) to (h). In all these figures, resonances manifest themselves as reflection maxima correlated with transmission minima. A slow decrease (resp. increase) of the transmission level (resp. reflection level) is also observed at low frequencies for the parallel polarization. This latter evolution can be readily attributed to the plasmon-like band associated to the periodic array of continuous wires [Pendry, 1998].

For the parallel polarization and the structures with the SRRs of larger sizes (structures 1 and 2), two resonances are observed within the spectral window of measurements [Figs. 12(a) and 12(b)]. Only the first resonance is experimentally observed for structures 3 and 4. The SRR resonances actually shift towards higher and higher frequencies as the whole SRR length is decreased. In the same time, their amplitude becomes smaller and smaller. For the first resonance, the maximum reflection R_{max} decreases from ~0.63 to ~0.5 while the minimum reflection R_{min} remains close to ~0.35 [Fig. 11(b)]. Accordingly, the minimum transmission T_{min} increases from ~0.12 to ~0.25 while the maximum transmission T_{max} remains close to ~0.6 [Fig. 11(a)]. It is worthwhile noticing that the values of R and T out of resonance correspond to those expected for a single face of silicon wafer partially covered with ~10-15% of highly reflecting metal. Whereas (R+T) approaches unity in this case ($R_{min}+T_{max}$~0.95), its smaller value at resonance ($R_{max}+T_{min}$~0.75) clearly indicates the presence of dissipative losses in metallic elements. The frequency positions of resonances, the values of R and T out of resonance, the values of (R+T) in general as well as the shapes of experimental curves in Figs. 12(a) and 12(b) are very well reproduced by numerical simulations [Figs. 12(c) and 12(d)]. The only discrepancy between experiments and simulations stems from the smaller amplitudes of resonances measured in experiments, especially those at high frequencies. The second resonance predicted at ~180 THz (λ ~ 1.7μm) for structure 3 is even not resolved in the experiments. Actually, minute deviations of the geometry from unit cell to unit cell and particularly residual surface roughness of the SRRs and continuous wires can explain the damping and inhomogeneous broadening of resonances as well as the increasing importance of these effects at high frequencies.

For the perpendicular polarization and for structures 1, 2 and 3, a single resonance is observed within the spectral range of measurements [Figs. 12(e) and 12(f)]. In contrast, no resonance is detected for the structure with cut wires. The evolution of the SRR resonance with the SRR length is actually similar to that observed for the parallel polarization. Smaller SRR lengths simultaneously lead to higher resonance frequencies and smaller resonance amplitudes. A good agreement is found between experimental results and numerical simulations [Figs. 12(g) and 12(h)]. Previous remarks made for the parallel polarization

apply to the perpendicular polarization. Minute deviations from unit cell to unit cell and surface roughness of metallic elements are likely to explain the broader resonances with smaller amplitudes observed in the experiments. The second resonances predicted for structures 1, 2 and 3 in the frequency region from 170 to 200 THz [Figs. 12(g) and 12(h) manifest themselves only as smooth maxima (resp. minima) in the measured reflection (resp. transmission) spectra of Fig. 12(f) (resp. Fig. 12(e)]. Supplementary measurements between 200 and 250 THz (not shown here) did not reveal any other resonance.

Figure 13 shows the distribution of the electric field calculated at the bottom surface of metallic elements for each of the resonant modes observed in Fig. 12. These results are in agreement with previous calculations reported by Rockstuhl et al. [Rockstuhl, 2006]. When the incident field is polarized parallel to the SRR gap, resonant modes possess an odd number of nodes along the entire SRR. This number is equal to one for the first resonance, while it is equal to three for the second resonance. The first resonance also identifies to the so-called LC resonance as defined in previous studies at microwave and far infrared frequencies [Katsarakis, 2004, Katsarakis, 2005]. It simply identifies to the dipolar mode in the case of the cut wire. When the incident field is polarized perpendicular to the gap, resonant plasmon modes possess an even number of nodes. The first resonant mode in this polarization thus exhibits one additional node as compared to the first resonance in the parallel polarization. This in turn requires higher energies of the light field to excite this mode. The frequency of the first resonant mode in the perpendicular polarization is typically two times higher than that of the first resonant mode in the parallel polarization.



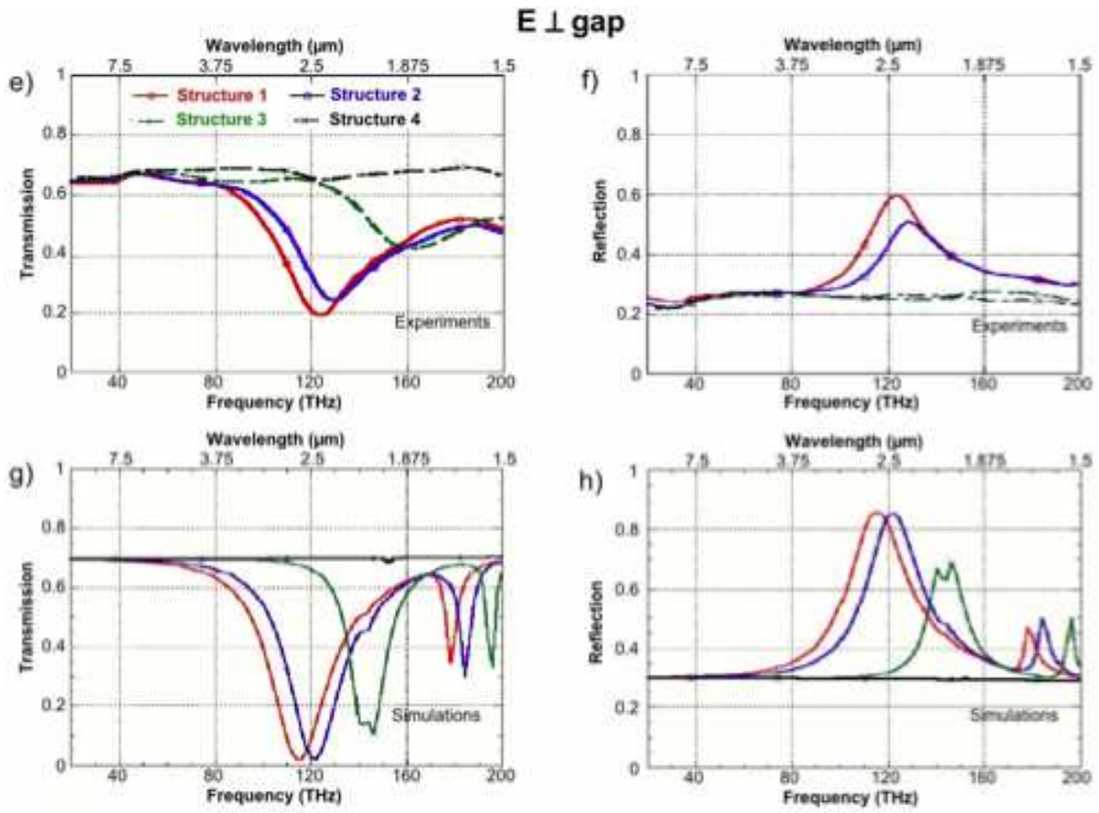


Fig. 12. Measured and simulated transmission/reflection spectra of the four structures depicted in Fig. 10. Curves in red, blue, green and black are for the 1st, 2nd, 3rd and 4th structures, respectively. – (a) and (b): transmission and reflection spectra measured for the parallel polarization (incident electric field parallel to the SRR gap). – (c) and (d): numerical simulations corresponding to (a) and (b), respectively. – (e) and (f): transmission and reflection spectra measured for the perpendicular polarization (incident electric field perpendicular to the SRR gap). – (g) and (h): numerical simulations corresponding to (e) and (f), respectively.

3.1.3 Frequency positions of resonances

At this stage, it is interesting to compare the frequency positions of resonances reported in Figs. 12 to those reported in previous works for similar structures with gold SRRs on glass substrate. For instance, the first resonance calculated in [Rockstuhl, 2006] for the parallel polarization and U–shaped SRRs with 400 nm long base and 190 nm long legs was found to be close to 3800 cm^{-1}, i.e. close to 115 THz instead of 65 THz measured in our experiments for U-shaped SRRs with similar sizes [Figs. 12(a), 12(b), and Fig. 13(b)]. The first resonance calculated in [15] for the parallel polarization and U-shaped SRRs with the same base but with 110 nm legs was found to be near 4800 cm^{-1}, i.e. near 144 THz instead of 80 THz measured in our experiments [Figs. 12(a), 12(b) and Fig. 13(c)]. Actually, all the mode frequencies calculated in [15] are 1.7- 1.9 times higher than those reported in this work, whatever the resonance order and the field polarization are. Approximately the same ratio is obtained when comparing the first resonance measured in [10] for SRRs of standard shape

(~100 THz) to that reported in Fig. 12(a) (~60 THz) for standard SRRs with the same total length (lm ~960 nm). This ratio is actually of the same order of magnitude than the ratio between the refractive index of glass and that of silicon. This suggests that in our case the electromagnetic field at resonance largely extends into the silicon substrate.

3.1.4 Coupling effects between continuous wires and SRRs

In the previous sections, it has been implicitly assumed that the presence of continuous wires had no influence on the resonant response of the structures except for a slow decrease of the transmission observed at low frequencies for the parallel polarization. However, a careful examination of the field distributions in Fig. 13 indicates that, at least for the second resonance, the electromagnetic field extends well in the region comprised between the SRR and the closest wire. We thus performed a numerical analysis to investigate in more detail the possible existence of coupling effects between the SRRs and continuous wires. For this purpose, the spectral responses of the four structures were calculated for different distances d between the SRR base and the closest wire. They were also compared to the spectral response of a periodic array of SRRs only.

Results of our calculations are shown in Figs. 14(a) and 14(b) for structure 1 with three values of d, for a periodic array of SRRs without continuous wires and for a periodic array of wires without SRRs. The dimensions of SRRs are the same for the first four structures. The lattice period is identical for all the structures. Calculations are performed within the same spectral range as in Fig. 12, and the incident electric field is polarized parallel to the continuous wires and/or to the SRR gaps. Figure 14(a) represents the transmission spectra calculated for the different structures. Figure 14(b) shows the electric field distributions calculated for the different resonances observed in Fig. 14(a). As seen in Fig. 14(a), the position of the first SRR resonance is not modified by the presence of the continuous wires whatever the separation between SRRs and wires is. Only the shape of the resonance is modified, and it becomes asymmetric with the presence of the wires.

This asymmetry mainly results from the fact that the optical response of the wires [pink dashed curve in Fig. 14(a)] adds to that of the SRRs. A weak coupling between SRRs and wires only occurs at the smallest separations between the two metallic elements as shown from the calculated distribution of the electric field at the first SRR resonance (Fig. 14(b), second column).

The evolution of the second SRR resonance is quite different. For a sufficiently large separation between the SRRs and wires ($d \geq 100$ nm), the frequency position of this second resonance is still rather independent of the presence of the wires. This justifies our previous interpretations concerning the results of Fig. 12, where the different spectra were obtained for $d \approx 130$ nm. However, for small separations between the SRRs and wires, strong coupling effects exist, which lead to a splitting of the second SRR resonance into two components [Fig. 14(a)]. These components are well separated for the smallest value of d (black dashed curve in Fig. 14(a), $d = 10$ nm). As seen in Fig. 14(b) (second and third columns), the modal field of the low frequency component is found to be concentrated in the region between the SRR base and the closest wire. That of the high frequency component is rather concentrated in the SRR legs.

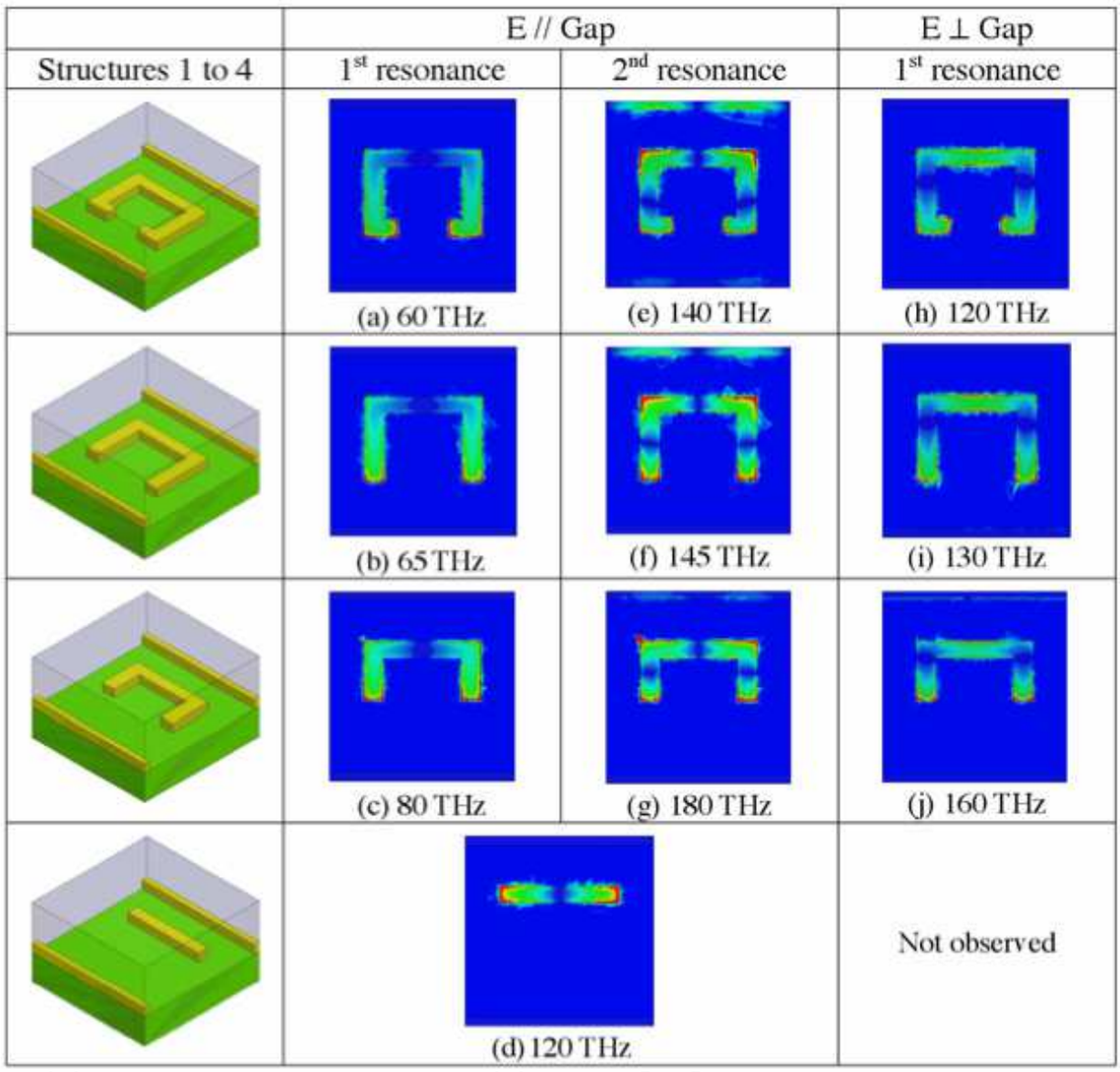


Fig. 13. Magnitude of the normal electric field component (|Ez|) calculated at the bottom surface of the metallic elements for each of the resonant plasmon modes observed in the different spectra of Fig. 11. The different colours, from blue to red correspond to increasing magnitudes of the field component. Modes are classified according to the resonance order and to the polarization of the incident electric field. As expected, both the energy and the number of field nodes increase with the resonance order.

Calculations above were repeated for structures with U-shaped SRRs as structures 2 and 3 and for structures with cut wires as structure 4 (Fig. 11). The same behavior was found in the case of structures with U-shaped SRRs. The frequency position of the first resonance was not modified when the distance between SRRs and continuous wires was varied. The second resonance split into two components for small values of d. In contrast, the structures with cut wires did not exhibit the same "robustness" of the first resonance against coupling effects.

The resonant mode split into two distinct components when the separation between cut wires and continuous wires was smaller than 50 nm. This different behavior can be simply explained by the fact that unlike structures with true SRRs, the field of the first resonant mode is obviously concentrated in the close neighbourhood of the continuous wires, i.e. in the cut wires themselves.

Coupling effects were also investigated from numerical simulations for the perpendicular polarization. We only considered the first SRR resonance since it was the only one clearly observed in the experiments (Fig. 12). The frequency position of this resonance was found to be rather independent of the presence of continuous wires whatever the separation between the SRRs and wires was. However, a small splitting of the resonance was observed for very small separations (d = 10 nm) in the case of U-shaped SRRs with small legs (structure 3).

3.1.5 Metamaterials with negative refraction on silicon

It is now well established that the use of an array of continuous metallic wires allows obtaining a negative permittivity over the whole plasmon-like band when the electric field is polarized parallel to the wires [Pendry, 1998]. Figures 12 and 14(a) presently show that this band can extend well up to near-infrared frequencies for a sufficiently small period of the wire lattice. On the other hand, it has been demonstrated that an array of metallic SRRs can exhibit a magnetic response in the optical domain with a negative permeability at certain frequencies [Enkrich, 2005]. However, this situation only occurs at SRR resonances and for an oblique or grazing incidence, i.e. for an incident magnetic field with a non-zero component along the SRR axis. An additional condition is that the resonant plasmon mode must possess an odd number of field nodes along the SRR [Shalaev, 2005]. Concerning this latter aspect, our experimental results confirm that the first resonant mode, the so-called LC resonance, is by far the most exploitable due both to its strength and to its robustness against parasitic coupling effects. They also show that its frequency position can be finely tuned by adjusting the total length of SRRs and using for instance U-shaped SRRs. One solution to achieve a magnetic response at normal incidence with respect to the sample plane consists in using a stack of SRR layers [Liu, 2008] or simpler, a stack of cut-wires as originally proposed in [Shalaev, 2005]. Coupling between adjacent SRRs or between adjacent cut-wires leads to the formation of hybridized plasmon modes of opposite symmetry. Anti-symmetric plasmon modes can exhibit a magnetic response, and lead to a negative permeability in certain frequency regions. Our experimental results in Fig. 12 show that the resonance associated to the dipolar mode of cut-wires is well pronounced for the fabricated structures. Coupling between two such modes in a multilayer stack should thus allow obtaining a magnetic response at normal incidence. One advantage in using stacked cut-wires instead of stacked SRRs stems from the possibility of achieving more easily a magnetic response at (high) near- infrared frequencies. This is all the more true when metallic nanostructures are fabricated on a high permittivity substrate such as silicon. All the plasmon resonances are shifted to low frequencies, and the realization of very-small-size SRRs operating at telecommunication wavelengths on silicon would require pushing the lithographic techniques to their present limits.

3.2 Optical asymmetric cut-wire pairs

3.2.1 Negative refractive index in optical asymmetric cut-wire pairs

In the previous structures, SRRs were associated with continuous wires to obtain negative index at infrared wavelengths. In this chapter we will study asymmetric cut-wire pairs to obtain also negative index. Metallic nanostructures can be regarded as elementary circuits including nano-capacitors, inductors or resistors [Engheta, 2007]. The simplest resonator that can be imagined is a dipole consisting of a simple metallic cut-wire. Coupling two such oscillators lead to two eigenmodes with opposite symmetry. The virtual current loop of the anti- symmetric mode is now recognized as a mean to create artificial magnetism at optical frequencies [Grigorenko, 2005, Shalaev, 2005]. Fig. 15 shows the structure under consideration. It consists of a periodic array of paired cut-wires separated by a dielectric layer. For simplicity the spacer has been taken to be silicon dioxide (SiO2) with a dielectric permittivity $\varepsilon_r = 2.25$ and a thickness of 100 nm. The surrounding medium is air with $\varepsilon_r = 1$. The relevant polarization of the impinging light is given in Fig. 15(a) with the electric field parallel to the longest side of the cut- wires. Transmission spectra are presented in Fig. 15(b). All the simulations are done using a commercial finite element code (HFSS, 2006). An array of isolated cut-wires is actually found when the separation distance between cut-wires is large: only one resonance (the dipolar mode) is observed in this case (red curve in Fig. 15(b)). This response can be interpreted in terms of a localized plasmon resonance [Rockstuhl, 2006, Kante, 2008]. When the separation distance between cut-wire pairs is progressively diminished, the response of the paired system is modified due to the interaction between its elementary constituents.

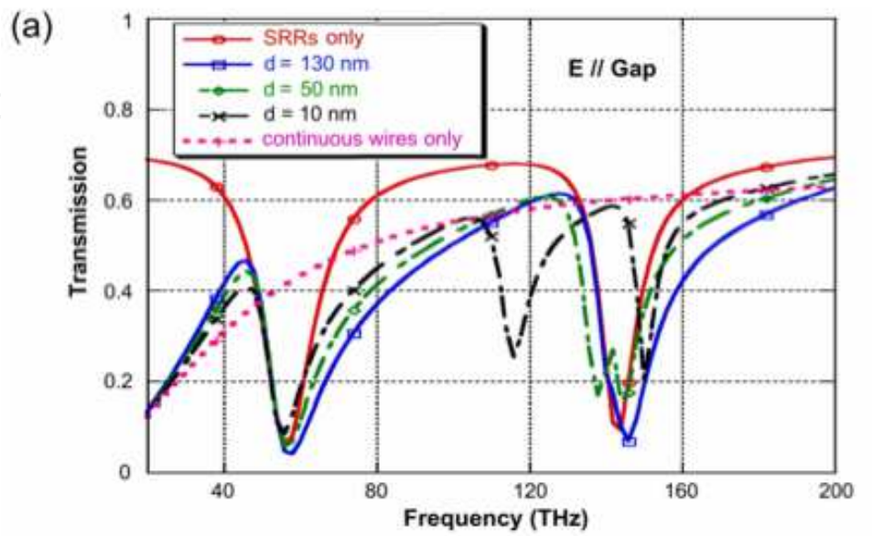
Following the plasmon hybridization concept [Kreibig, 1981, Prodan, 2003], coupling effects lift the degeneracy of the single cut-wire mode, thus leading to two distinct plasmons modes [Liu, 2007, Kante 2009], the anti-symmetric and symmetric modes as shown in Fig. 15(b) (blue curve). The symmetric mode with larger restoring force is at a higher energy than the anti-symmetric mode. The main idea of our work is to invert this process. The symmetric mode, which easily couples to incident light, corresponds to a wide rejection band with negative permittivity. The anti-symmetric mode, which is difficult to excite due to the opposite contributions of the two dipoles, manifests itself as a small transmission dip with negative permeability. Achieving such a resonance at a higher frequency than the symmetric mode will ease the overlap condition as proposed recently in [Kante, 2009, Sellier, 2009]. For this purpose, one solution is to break the symmetry of the cut-wire pair. This is achieved in Fig. 15(d) by displacing one of two cut-wires in the direction of the electric field.

Fig. 16(a) and (b) shows the evolutions of the resonant modes and transmission spectra with the longitudinal shift dx between the two cut-wires of each pair. Simulations are performed in the infrared domain. As a major result, for a sufficiently large displacement dx (here dx > 350 nm), the hybridization scheme is inverted with the symmetric mode at a lower frequency than the anti-symmetric mode. The two hybridization schemes are presented in Fig. 15(c) and (e), respectively. Fig. 16(d) clearly shows that a negative refraction regime is obtained (between 145 and 160 THz for dx = 600 nm) for the inverted scheme while the index of refraction remains always positive (dx = 0 nm) for the normal hybridization case (Fig. 16(c)). This extends to infrared frequencies previous results reported by the authors at

microwave frequencies [Kante, 2009, Sellier, 2009]. As seen in Fig. 16(d), negative refraction corresponds to an overlap between the region with negative permittivity and that with negative permeability. It is worthwhile noticing that the domain of overlap with negative permittivity and permeability can be controlled through the different degrees of freedom of the structure [Kante, 2009].

3.2.2 Hybridization of the localized plasmons of SRRs

The recipe proposed above for obtaining a negative index with plasmon hybridization can be applied to any structure supporting localized plasmons. The inversion process resulted from a radical change in near field Coulomb interactions between cut-wires in each pair [Kante, 2009, Christ, 2008]. Let us consider for instance a periodic array of paired SRRs, which are fundamental building blocks in the design of metamaterials. Indeed, the use of SRRs has allowed the achievement of negative magnetic permeability, which is impossible with natural materials at high frequencies. However, obtaining a negative magnetic permeability requires the incident wave to possess a magnetic component along the SRR axis. Such a requirement is not easily fulfilled in optics [Dolling, 2006, Liu, 2009]. Moreover, the electromagnetic response of SRRs has been shown to saturate at optical frequencies [O'Brien, 2002]. In most experimental works reported so far in the infrared domain, normal incidence has been used instead of a grazing or oblique incidence [Kante, 2008]. In this situation, only the electric field can couple to the structure. SRR resonances are nothing but plasmonic resonances which can be classified into even and odd modes depending on the polarization the exciting light with respect to the structure [20]. While even modes are excited for an incident electric field perpendicular to the SRR gap, odd modes are excited for an electric field parallel to this gap. It is straightforward to see that only odd modes can lead to a magnetic moment or eventually to a negative permeability under oblique incidence.



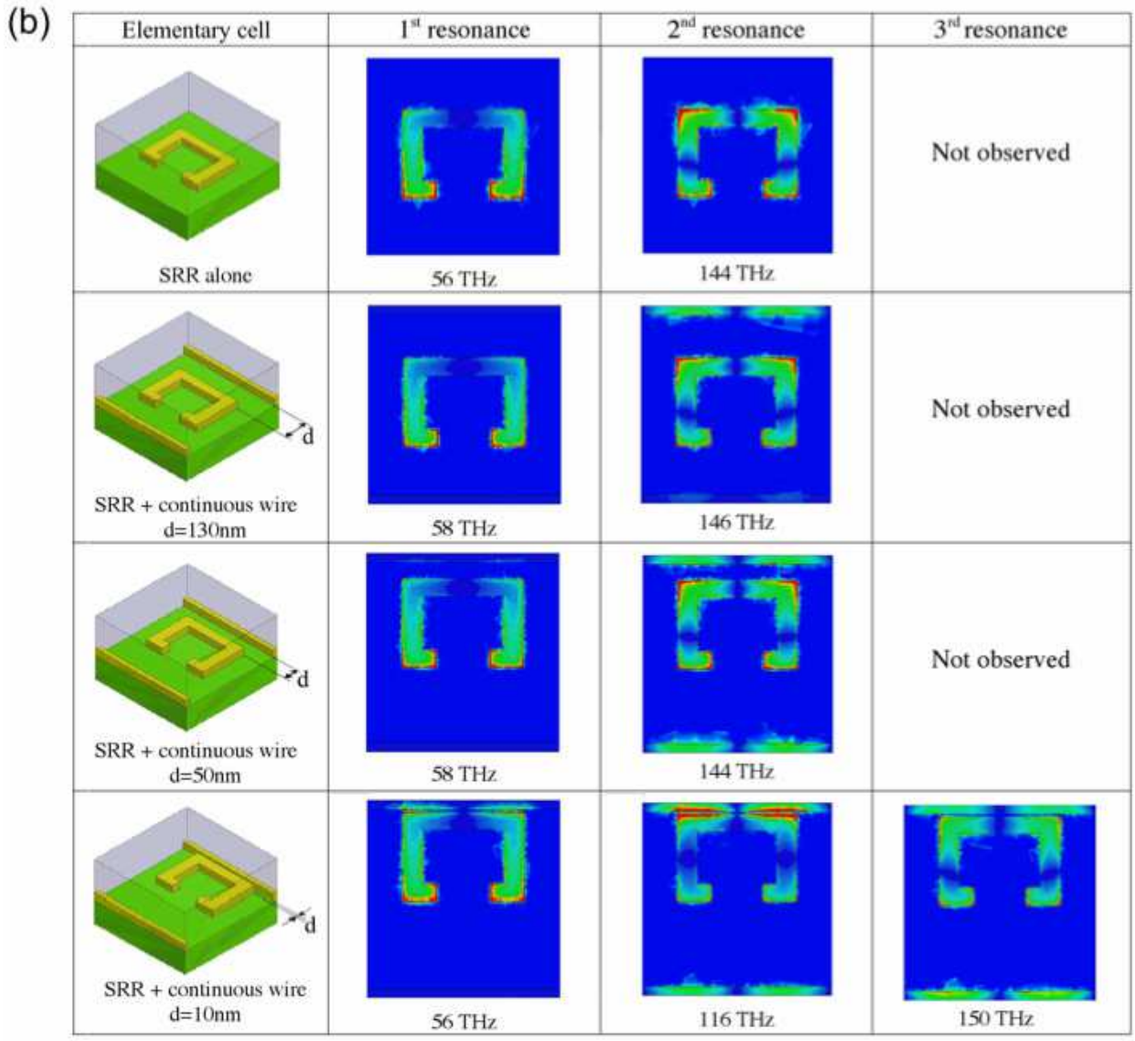


Fig. 14. (a) Transmission spectra calculated for a periodic array of SRRs (red curve), a periodic array of continuous wires (pink dashed curve) and periodic arrays of SRRs and wires with different separations between SRRs and wires: d=130 nm (blue curve), d=50 nm (green dashed curve), d=10 nm (black dashed curve). In each case, the incident electric field is polarized parallel to the gap, the SRR dimensions and lattice period as the same as for structure 1 in Fig. 10. (b) Magnitude of the normal electric field component (|Ez|) calculated at the bottom surface of the metallic elements for each of the resonant modes observed in the transmission spectra of Fig. 14 (a). The different colours, from blue to red correspond to increasing magnitudes of the field component. Modes are classified according to the resonance order and to the separation d between the SRR and the closest wire.

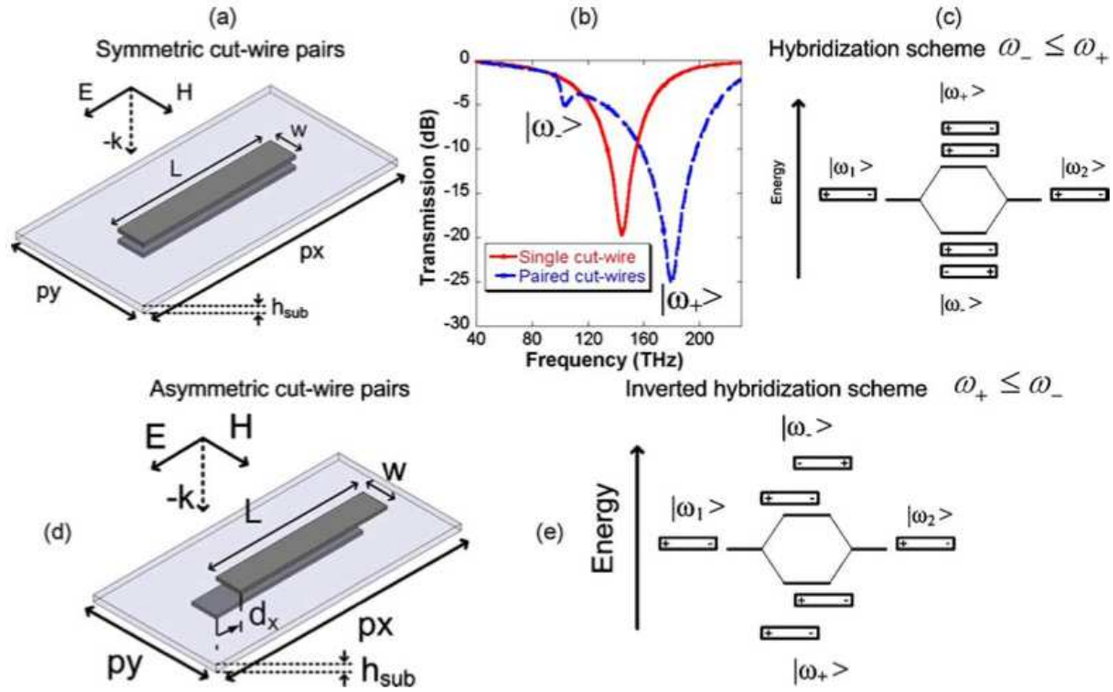


Fig. 15. (a and d) Schematics of the symmetric and asymmetric cut-wire pairs, respectively. (b) Transmission of an array of un-coupled or coupled cut-wires structure with p_x=1.2mm, p_y=200nm, p_z=600nm, w=30nm, L=600nm, h_{sub} =100nm and ε_{sub} =2.25. The pieces of gold metals are described by a Drude model whose parameters can be found in [Kante, 2008]. (c and e) Hybridization scheme and inverted hybridization scheme, respectively.

Fig. 17 (red curves) presents transmission spectra of a single SRR layer designed to operate in the infrared range for two polarizations at normal incidence. When the electric field is perpendicular to the gap, only one resonance (the fundamental even mode) is observed in the frequency range of interest while two resonances are observed for the parallel polarization. These last two resonances respectively correspond to the first and second odd plasmonic modes [Rockstuhl, 2006, Kante, 2008], the fundamental mode being also called LC resonance. When two such SRR structures are brought close to each other, the localized plasmons can hybridize according to a plasmon hybridization scheme similar to the one previously described for cut-wire pairs (Fig. 15). In what follows, the hybridization scheme of an SRR pair is analyzed for both parallel and perpendicular polarization as well as for resonances of different orders. As it will be shown, a negative index of refraction can be obtained at normal incidence for a periodic structure, which is exclusively made of SRRs and based on an inverted hybridization scheme. The SRR pair forming the elementary motif of the periodic structure is depicted in Fig. 17 (left graph). As seen, the lower SRR of the pair is shifted in the x and y directions with respect to the upper one. Following our previous work on cut-wire pairs, this configuration will be simply called ''asymmetric SRR pair''. A system of coupled SRRs has been recently investigated by Liu et al. [Liu, 2009], but in a twisted configuration. These authors showed that the twist angle between vertically coupled SRRs could modify either the electric or magnetic response of the system resulting in what they called a ''stereometamaterial''. Our structure can thus be regarded as a particular

''stereometamaterial''. In contrast, rotating one SRR with respect to another did not produce any inverted hybridization scheme, while this scheme is the most appropriate one for obtaining negative refraction. In fact, split ring resonators are complex structures regarding their responses to an electromagnetic field since they support localized plasmons addressable either by the electric field or the magnetic field. To our knowledge, using the two degrees of freedom (dx, dy) in the design of the SRR pair (Fig. 17 (left graph)) to achieve a negative index of refraction has never been reported so far in the context of SRR-based metamaterials.

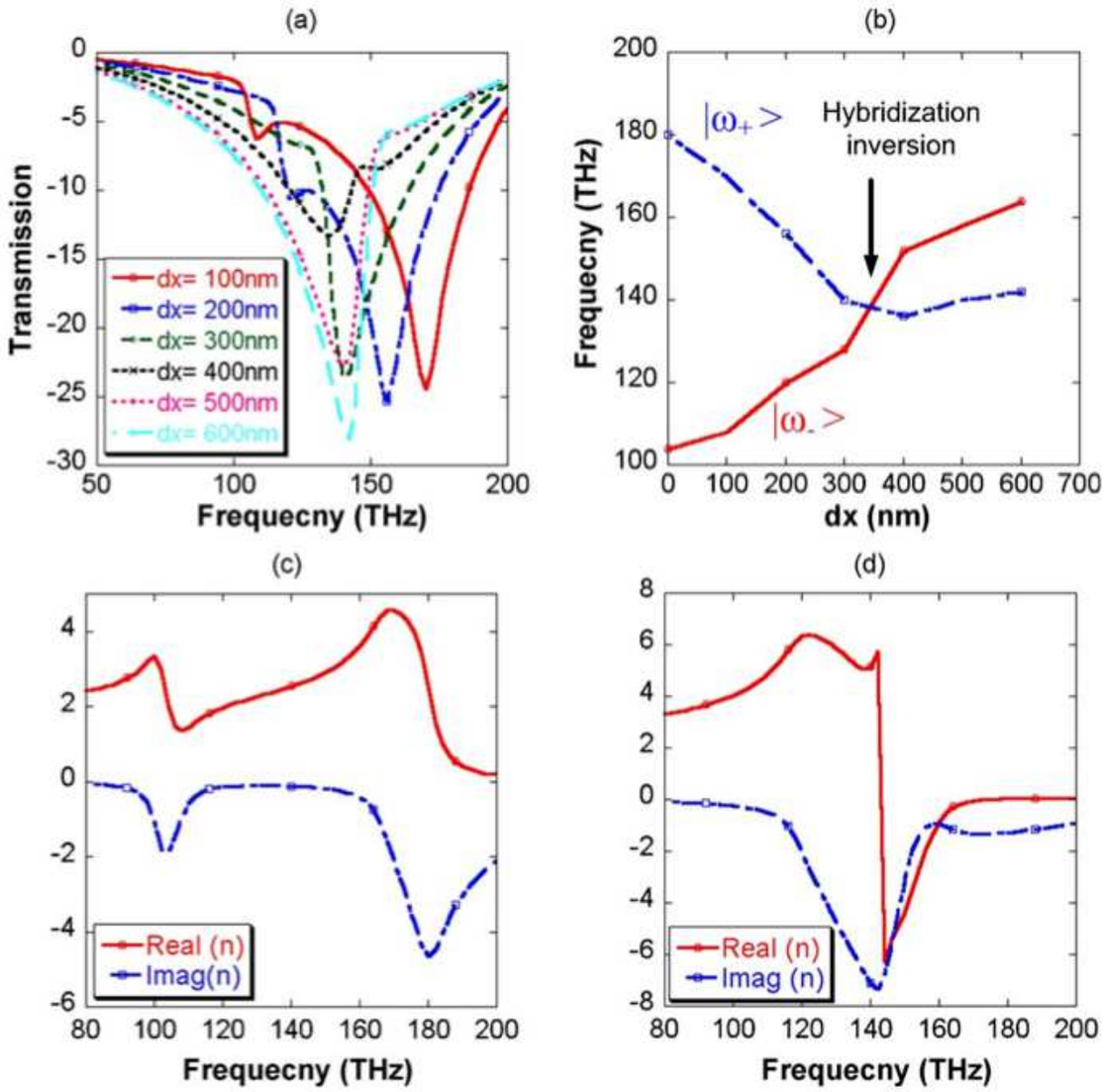


Fig. 16. (a) Transmission spectra of the two-dimensional array of asymmetric cut-wire pairs calculated for different values of the longitudinal shift (dx) between the two cut-wires in each pair. (b) Evolutions of the symmetric and anti-symmetric mode frequencies as a function of the dx shift. (c) Effective index of refraction [30] calculated for dx = 0 with a de-embedding up to the metamaterials interfaces. (d) Same type of calculations for dx = 600 nm.

3.2.3 Hybridization of the LC resonance

The LC resonance (i.e. the fundamental odd mode) is excited at normal incidence when the electric field is parallel to the gap. This resonance has been experimentally observed from microwaves to optics. Electric charges in metallic SRR arms are mainly located near the SRR gap (insert of Fig. 17, middle graph). Fig. 18 shows the modifications of the transmission spectrum when coupling vertically two SRR layers. Curves in the left graph correspond to different values of dx at a fixed dy (dy = 0). Curves in the right graph correspond to different values of dy at fixed dx (dx = 0). As expected, in all cases, coupling between SRRs splits the LC resonance in two eigenmodes. The symmetric mode, which has the largest amplitude, is found at the highest frequency for dx = dy = 0. In principle, a longitudinal magnetic coupling also exists [Liu, 2009], but can be neglected for a qualitative understanding of the hybridization scheme in presence of electric coupling. As seen in the left graph of Fig. 17, a shift of one of the two SRRs in the direction perpendicular to the gap (dx≠0) has a weak influence. One just observes a small decrease of the mode amplitudes. The evolution is radically different when the shift occurs in the direction parallel to the gap (dy ≠ 0). An inversion of the hybridization scheme is observed for sufficiently large values of dy. The overall results obtained for the LC mode of SRRs are then very comparable to those reported for the dipolar mode of cut-wires. The LC mode exhibits indeed a dipole-like behavior.

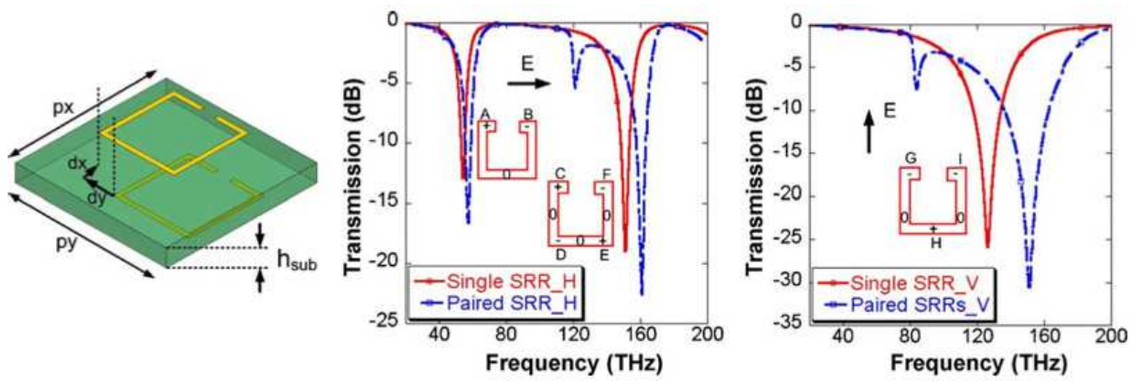


Fig. 17. (Left) Schematics of the asymmetric SRR pair. (Middle) Transmission spectra of periodic SRR arrays at normal incidence for a field polarization parallel to the SRR gap. (Right) Transmission spectra of periodic SRR arrays for a field polarization perpendicular to the SRR gap. In the middle and right graphs, red curves are for one-SRR-layer array while blue curves are for a two-layer array of paired SRRs. Inserts show the distributions of charges and electric field nodes for the different resonances in the one-layer array. Squared SRRs are used with 700 nm side length and 200 nm gap width. The 100 nm wide conducting elements are described using the Drude model reported in [Kante, 2008]. Other parameters are: px = py = 1.4 mm, pz = 1 mm, hsub = 100 nm, εsub = 2.25.

3.2.4 Hybridization of the second odd plasmonic mode

Let us now consider the second odd mode. The corresponding distribution of electric charges and field nodes in SRR arms is shown in the middle graph of Fig. 17 (right insert) for a one-layer SRR array. This picture shows that this mode has a ''dipole activity'' in both the x and y directions. Charges at the extremities of CD and EF arms produce the dipolar activity along the x direction while those at the extremities of the DE arm produce the dipolar activity along the y direction. Correspondingly, in a two-layer SRR array, an inversion of the hybridization occurs whether one of the two layers is displaced along the x or the y direction (Fig. 18). In each case, the inversion stems from the near field interaction between the active dipoles in the corresponding direction. In the case of a displacement along x, the inversion results from the interaction of dipoles CD and EF with dipoles C′D′ and E'F'. The primes referring to the second SRR. In the case of a displacement along y, it results from the interaction between DE and D′E′.

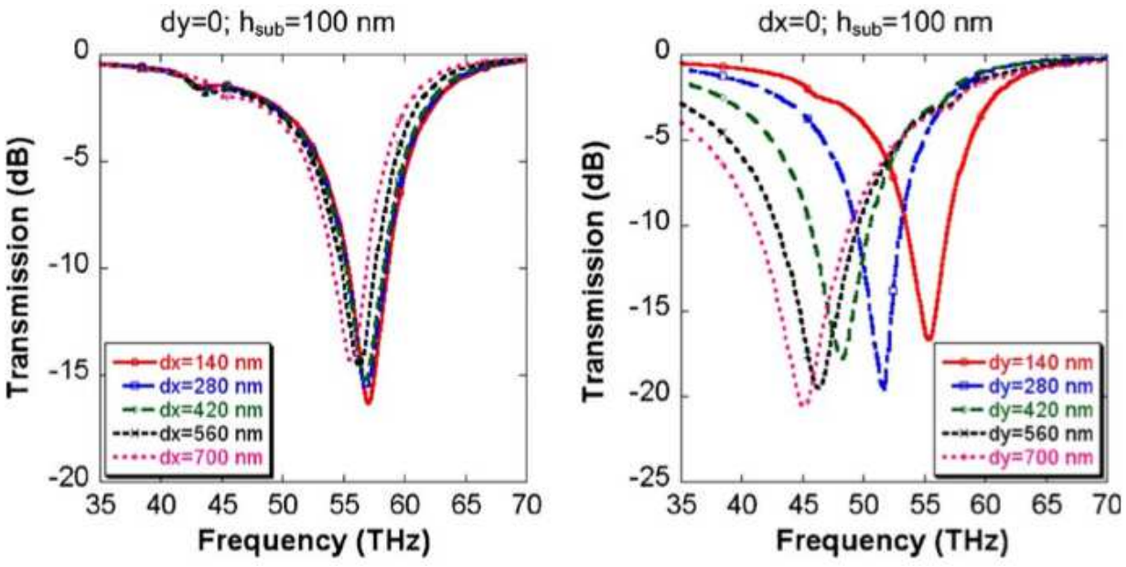


Fig. 18. Transmission spectra of a periodic array of asymmetric SRRs pairs around the LC resonance for different values of dx at dy=0 (left) and for different values of dy at dx = 0 (right)

3.2.5 Hybridization of the fundamental even plasmonic mode (perpendicular polarization)

When the incident electric field is perpendicular to the gap, the SRR can be regarded as two cut-wires in parallel since the charges in the two arms GH and IH oscillate in phase (see insert in the right graph of Fig. 17). In consequence, the hybridization of localized plasmons evolves a priori as in the case of cut-wires pairs [Kante, 2009]. Therefore, only a displacement along the x direction (parallel to the dipoles GH and HI) for one of the SRRs of the asymmetric pair can lead to an inverted hybridization scheme with the possibility of a negative index of refraction.

The inversion of the hybridization scheme for dx ≠ 0 is illustrated from calculated transmission spectra in Fig. 20(a). Results of calculations for the effective index of refraction

are presented in Fig. 20(c) and (d) for a symmetric SRR pair (dx = dy = 0) and an asymmetric pair (dx = 700 nm, dy = 0), respectively. Results obtained for the symmetric pair are comparable to those reported in [Liu, 2008]. There with no overlap between the regions of negative epsilon and negative mu. In contrast, a negative index of refraction is clearly obtained for the asymmetric SRR pair in Fig. 20(d).

Results obtained for a transversal displacement (dy ≠ 0) of one SRR of the pair may appear to be quite surprising since three peaks are observed in the transmission spectra instead of two (Fig. 20(b)). However, a careful analysis reveals that these peaks have different origins. Three types of dipole–dipole interactions are indeed involved: GH with G'H', GH with I'H' and IH with G' H'. For an intermediate value of dy (i.e. dy = py/2 = 350 nm), the dipole–dipole interactions GH - G'H' and I'H' - IH become degenerate, thereby leading to the disappearance of one of the three peaks.

In conclusion we have numerically demonstrated that the coupling between localized plasmons in periodic arrays of paired cut-wires or SRRs can be controlled by modifying the symmetry of each individual pair. It has been shown that breaking the symmetry of cut-wire or SRR stacks can lead to a negative index of refraction. The scheme proposed here contrasts with previous designs of negative index metamaterials where two kinds of meta-atoms were mixed. Only one type of meta-atom supporting localized plasmons is used. A true negative index band is achieved provided that the coupling between localized plasmons is appropriately controlled.

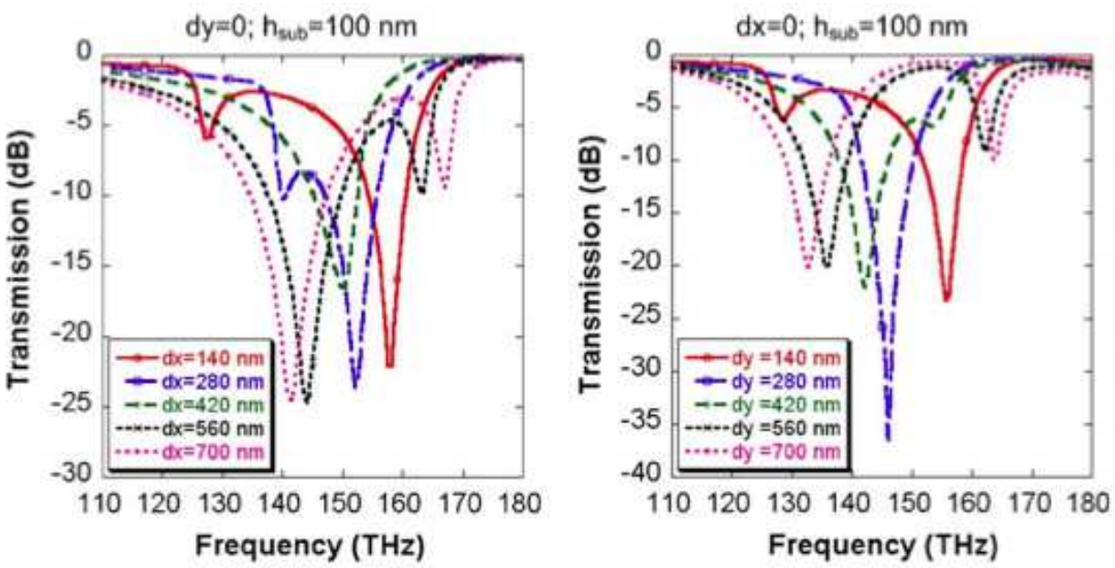


Fig. 19. Transmission spectra of a periodic array of a symmetric SRRs pairs around the second odd SRR mode for different values of dx at dy=0 (left) and for different values of dy at dx = 0 (right).

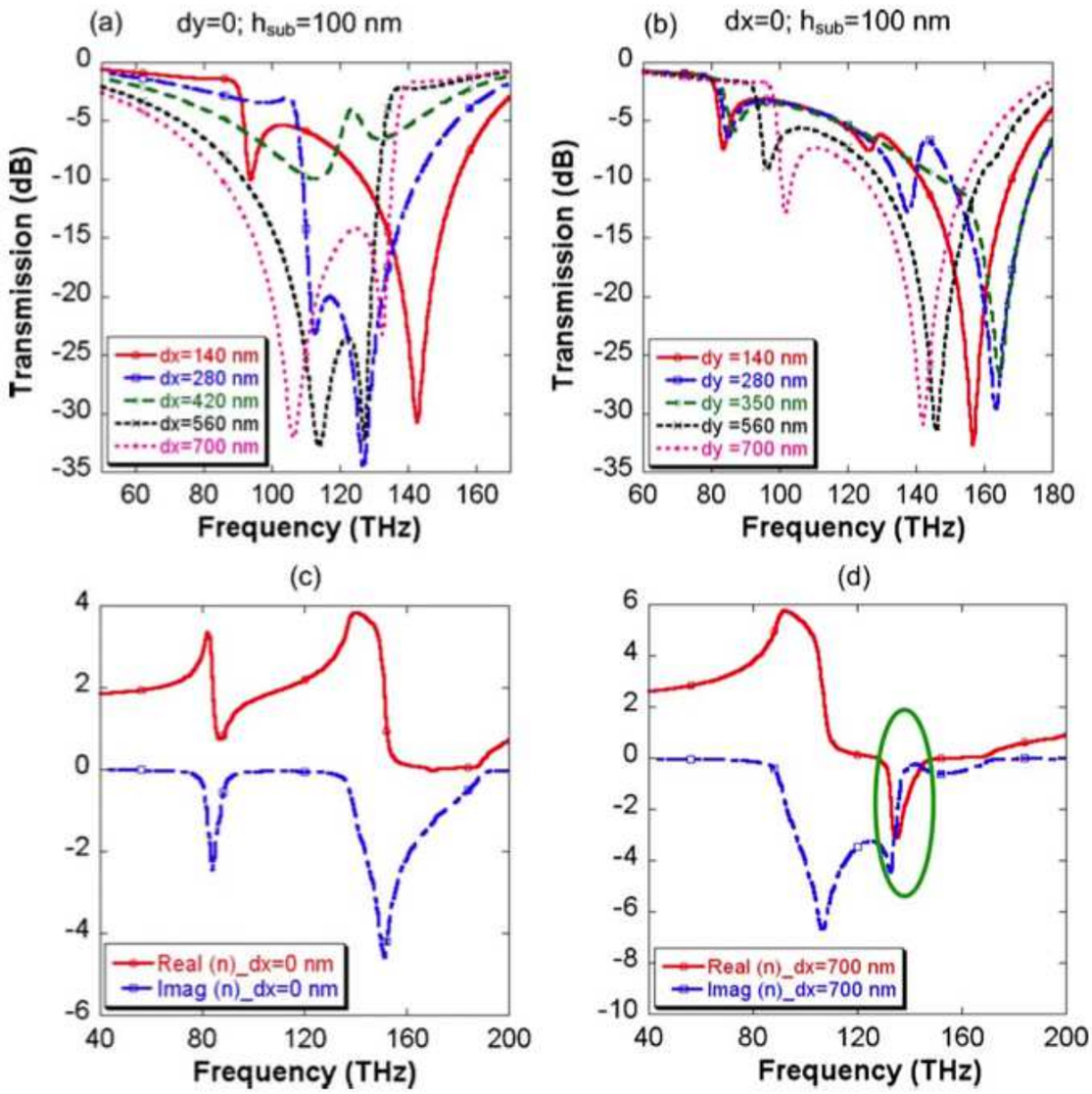


Fig. 20. (Top) Transmission spectra of a periodic array of asymmetric SRRs pairs for vertical polarization and different values of dx at dy=0 (a) and for different values of dy at dx = 0 (b). (Bottom) Effective index of refraction (real and imaginary parts) calculated for dx = 0 and dy = 0 (c) and for dx = 700 nm, dy = 0 (d), pz = 1 mm with a de-embedding up to the metamaterials interfaces.

4. Conclusions

In this chapter, we have presented different metamaterials with a negative index at microwave and optical frequencies. Through numerical simulations and measurements, we have shown that it was possible to obtain a negative index by optimizing the coupling between different layers of metamaterials. We have also shown that this concept can be implemented from microwaves to optics. These works are believed to open a new way for the design of negative refraction metamaterials from microwaves to optics.

5. References

Aydin, K., Bulu, I., Ozbay, E., (2005), Focusing of electromagnetic waves by a left-handed metamaterial flat lens, *Optics Express,* Vol.13, n°22, pp.8753-8759.

Burokur, S. N. , Latrach, M., Toutain, S., (2005), Theoretical investigation of a circular patch antenna in the presence of a left-handed medium, *IEEE Antennas and Wireless Propagation Letters* Vol.4, pp.183-186.

Burokur, S. N., Sellier, A., Kanté, B., de Lustrac, A., (2009a), Symmetry breaking in metallic cut wire pairs metamaterials for negative refractive index, *Applied Physics Letters,* Vol.94, 201111.

Burokur, S. N., Lepetit, T., de Lustrac, A., (2009b), Incidence dependence of negative index in asymmetric cut wire pairs metamaterials, *Applied Physics Letters* Vol.95, 191114.

Cai, W. , Chettiar U. K., Kildishev A. V., Shalaev V. M., (2007), Optical cloaking with metamaterials, *Nature Photonics* Vol.1, pp.224-227.

Christ, A., Ekinci Y., Solak H. H., Gippius N. A., Tikhodeev S. G., Martin O. J. F., (2007), Controlling the Fano interference in a plasmonic lattice*, Physical Review B,* Vol.76, 201405□R.

Christ, A., Marin O.J.F., Ekinci Y., Gippius N. A., Tikhodeev S. G., (2008), Symmetry Breaking in a Plasmonic Metamaterial at Optical Wavelength, *Nano Letters,* Vol.8, pp.2171-2175.

Dolling, G. , Enkrich C., Wegener M., Zhou J. F., Soukoulis C. M., Linden S., (2005), Cut-wire pairs and plate pairs as magnetic atoms for optical metamaterials, *Optics Letters,* Vol.30, n°23, pp.3198-3200.

Dolling, G., Enkrich C., Wegener M., Soukoulis C. M., Linden S., *(2006),* Simultaneous Negative Phase and Group Velocity of Light in a Metamaterial, *Science*, Vol.312, pp. 892-894.

Enkrich, C. , M. Wegener, S. Linden, S. Burger, L. Zschiedrich, F. Schmidt, J. F. Zhou, Koschny, T., Soukoulis, C. M., (2005) , Magnetic Metamaterials at Telecommunication and Visible Frequencies, *Physical Review Letters* Vol.95, 203905.

Gaillot, D. P., Cröenne, C., Lippens, D., (2008), An all-dielectric route for terahertz cloaking, *Optics Express,* Vol.16, n°6, pp.3986-3992

Grigorenko, A.N., Geim A. K., Gleeson H. F., Zhang Y., Firsov A. A., Khrushchev I. H., Petrovic J., (2005), Nanofabricated media with negative permeability at visible frequencies, *Nature,* Vol.438, pp.335–338.

Gundogdu, T., F., Katsarakis N., Kafesaki M., Penciu R. S., Konstantinidis G., Kostopoulos A., Economou E. N., and Soukoulis C. M., (2008), Negative index short-slab pair and continuous wires metamaterials in the far infrared regime, *Optics Express*, Vol.16, n°12, pp. 9173-9180.

Guven, K., M. D. Kaliskan, and E. Ozbay, (2006), Experimental observation of left-handed transmission in a bilayer metamaterial under normal-to-plane propagation, *Optics Express,* Vol.14, n°19, pp. 8685-8693.

HFSS, High-frequency structure simulator version 10.1 Finite-element package, Ansoft Corporation, Pittsburgh, PA (2006).

Kanté, B., Ourir A., Burokur, S. N., Gadot, F., de Lustrac, A., (2008a), Metamaterials for optical and radio communication, *Comptes Rendus Physique,* Vol.9, n°1, pp.31-40.

Kanté, B., de Lustrac, A., Lourtioz, J. M., Burokur, S. N., (2008b), Infrared cloaking based on the electric response of split ring resonators, *Optics Express,* Vol.16, n°12, pp. 9191-9198.

Kanté, B., de Lustrac A., Lourtioz, J.M. , Gadot, F., (2008c), Engineering resonances in infrared metamaterials, *Optics Express*, Vol.16, n°10, pp. 6774-6784.

Kanté, B., Burokur, S. N., Sellier, A. , de Lustrac, A., Lourtioz, J.-M., (2009a), Controlling Plasmon Hybridization for Negative Refraction Metamaterials, *Physical Review B*, Vol.79, 075121.

Kanté, B., de Lustrac, A., Lourtioz, J. M., (2009b), In-plane coupling and field enhancement in infrared metamaterial surfaces, *Physical Review B,* Vol.80, 035108.

Katsarakis, N., Koschny T., Kafesaki M., Economou E. N., and C. M. Soukoulis, (2004), Electric coupling to the magnetic resonance of split ring resonators, *Applied Physics Letters,* Vol.84, pp.2943-2945.

Katsarakis, N., Konstantinidis, G., Kostopoulos, A., Penciu, R. S., Gundogdu, T. F., Kafesaki, M., Economon, E. N., Koschny, T., and Soukoulis, C.M., (2005), Magnetic response of split-ring resonators in the far- infrared frequency regime, *Optics Letters* Vol.30, pp.1348-1350.

Kreibig, U., Althoff, A., Pressmann, H., (1981), Veiling of optical single particle properties in many particle systems by effective medium and clustering effects, *Surface Science* Vol.106 , n°1-3, pp. 308-317.

Leonhardt, U., (2006), Optical Conformal Mapping, *Science,* Vol.312, pp.1777-1780.

Linden, S., Enkrich, C., Wegener, M., Zhou J., Koschny, T., Soukoulis, C. M., (2004), Magnetic Response of Metamaterials at 100 Terahertz, *Science,* Vol.306, pp.1351-1353.

Liu, N., Guo H., Fu L., Kaiser S., Schweizer H., Giessen H., (2007), Plasmon Hybridization in Stacked Cut-Wire Metamaterials, *Advanced Materials*, Vol.19, pp.3628-3632.

Liu, N., Guo H., Fu L., Kaiser S., Schweizer H., and Giessen H., (2008), Three-dimensional photonic metamaterials at optical frequencies, *Nature Materials* Vol.7, pp.31-37.

Liu, N., Liu H., Zhu S., Giessen H., (2009), Stereometamaterials, *Nat. Photon*. Vol.3, pp.157–162

Nicholson, A. M., Ross G.F., (1970), Measurement of the intrinsic properties of materials by time-domain techniques, *IEEE Transactions on Instrumentation And Measusrements* Vol.19, pp.377-382.

O'Brien S, Pendry J.B., (2002), Magnetic Activity at Infra Red Frequencies in Structured Metallic Photonic Crystals, *Journal of Physics Condensed Matter* Vol.14, pp.6383–6394.

Pendry, J. B. , Holden A. J., Stewart W. J., Youngs I, (1996), Extremely Low Frequency Plasmons in Metallic Mesostructures, *Physical Review Letters,* Vol.76, pp.4773-4776.

Pendry, J. B. , Holden A. J., Robbins D. J., Stewart W. J., (1999), Magnetism from conductors and enhanced nonlinear phenomena, *IEEE Trans. Microwave Theory Tech.*, Vol.47, pp.2075-2084.

Pendry, J. B. , (2000), Negative Refraction Makes a Perfect Lens, *Physical Review Letters,* Vol.85, pp.3966-3969.

Pendry, J. B., D. Schurig, and D. R. Smith, (2006), Controlling Electromagnetic Fields, *Science* Vol.312, pp. 1780-1782.

Prodan, E., C. Radloff, N. J. Halas, and P. Nordlander, (2003), A Hybridization Model for the Plasmon Response of Complex Nanostructures, *Science* Vol.302, pp. 419-422.

Rockstuhl, C., F. Lederer, C. Etrich, T. Zentgraf, J. Kuhl, and H. Giessen, (2006), On the reinterpretation of resonances in split-ring-resonators at normal incidence, *Optics Express,* Vol.14, n°19, pp. 8827-8836.

Sellier, A., Burokur S. N., Kanté B., de Lustrac A., (2009), Negative refractive index metamaterials using only metallic cut wires, *Optics Express*, Vol.17, 8, pp. 6301-6310.

Shalaev, V. M., Cai W., Chettiar U. K., Yuan H. K., Sarychev A. K., Drachev V. P., Kildishev A. V., (2005), Negative index of refraction in optical metamaterials, *Optics Letters* Vol.30, pp.3356-3358.

Shalaev, V. M. , (2007), Optical negative-index metamaterials, *Nature Photonics* Vol.1, pp.41-48.

Shelby, R. A. , D. R. Smith, and S. Schultz, (2001), Experimental Verification of a Negative Index of Refraction, *Science* Vol.292, pp.77-79.

Schurig, D., J. J. Mock, B. J. Justice, S. A. Cummer, J. B. Pendry, A. F. Starr, and D. R. Smith, (2006), Metamaterial Electromagnetic Cloak at Microwave Frequencies, *Science,* Vol.314, pp. 977-980.

Smith, D. R., Padilla W.J., Vier D. C., Nemat-Nasser S. C., Schultz S., (2000), Composite Medium with Simultaneously Negative Permeability and Permittivity, *Physical Review Letters,* Vol.84, pp.4184-4187.

Smith, D. R., Schultz S., Markos P., and Soukoulis C. M., (2002), Determination of effective permittivity and permeability of metamaterials from reflection and transmission coefficients, *Physical Review B* Vol.65, 195104.

Smith, D. R. , Pendry J. B., Wiltshire M. C. K., (2004), Metamaterials and Negative Refractive Index, *Science* Vol.305, pp.788-792.

Valentine, J., Zhang S., Zentgraf T., Ulin-Avila E., Genov D.A., Bartal G., Zhang X., (2008), "Three Dimensional Optical Metamaterial Exhibiting Negative Refractive Index," *Nature* Vol.455, pp.376-379.

Veselago, V. G. , (1968), The electrodynamics of substances with simultaneously negative values of e and μ, *Soviet Physics Uspieky* Vol.10, 509.

Wang, G., Fang J. R., Dong X. T., (2007), Refocusing of backscattered microwaves in target detection by using LHM flat lens, *Optics Express,* Vol.15, n°6, pp.3312-3317.

Yeh, P. , (1998), *Optical waves in layered media* (Wiley 1998).

Yen, T. J., Padilla W. J., Fang N., Vier D. C., Smith D. R., Pendry J. B., Basov D. N., Zhang X., (2004), Terahertz Magnetic Response from Artificial Materials, *Science* Vol.303, pp.1494-1496.

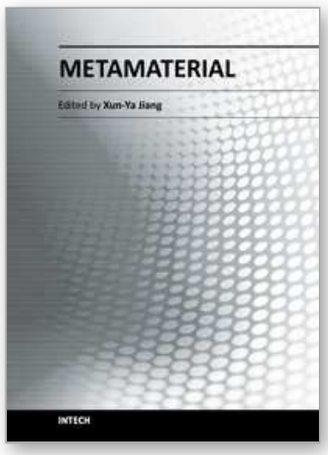
Zhang, S. , Fan W., Minhas B. K., Frauenglass A., Malloy K. J., Brueck S. R. J., (2005), Midinfrared Resonant Magnetic Nanostructures Exhibiting a Negative Permeability, *Physical Review Letters,* Vol.94, 37402.

Zhou, J., Zhang L., Tuttle G., Koschny T., Soukoulis C. M., (2006), Negative index materials using simple short wire pairs, *Physical Review B.* Vol. 73, 041101.

Zhou, J., Economon E., Koschny T., Soukoulis C. M., (2006), Unifying approach to left-handed material design, *Optics Letters* Vol.*31,* pp.3620-3622.

Zhou, J., Koschny T., and Soukoulis C. M., (2007), Magnetic and electric excitations in split ring resonators, *Optics Express,* Vol.15, pp.17881-17890 .

Ziolkowski, R.W., Kipple A., (2003), Application of double negative metamaterials to increase the power radiated by electrically small antennas, *IEEE Transaction Antennas Propag*ation Vol.51, pp.2626-2640.



Metamaterial

Edited by Dr. Xun-Ya Jiang

ISBN 978-953-51-0591-6
Hard cover, 620 pages
Publisher InTech
Published online 16, May, 2012
Published in print edition May, 2012

In-depth analysis of the theory, properties and description of the most potential technological applications of metamaterials for the realization of novel devices such as subwavelength lenses, invisibility cloaks, dipole and reflector antennas, high frequency telecommunications, new designs of bandpass filters, absorbers and concentrators of EM waves etc. In order to create a new devices it is necessary to know the main electrodynamical characteristics of metamaterial structures on the basis of which the device is supposed to be created. The electromagnetic wave scattering surfaces built with metamaterials are primarily based on the ability of metamaterials to control the surrounded electromagnetic fields by varying their permeability and permittivity characteristics. The book covers some solutions for microwave wavelength scales as well as exploitation of nanoscale EM wavelength such as visible specter using recent advances of nanotechnology, for instance in the field of nanowires, nanopolymers, carbon nanotubes and graphene. Metamaterial is suitable for scholars from extremely large scientific domain and therefore given to engineers, scientists, graduates and other interested professionals from photonics to nanoscience and from material science to antenna engineering as a comprehensive reference on this artificial materials of tomorrow.

How to reference

In order to correctly reference this scholarly work, feel free to copy and paste the following:

André de Lustrac, Shah Nawaz Burokur, Boubacar Kanté, Alexandre Sellier and Dylan Germain (2012). Design and Characterization of Metamaterials for Optical and Radio Communications, Metamaterial, Dr. Xun-Ya Jiang (Ed.), ISBN: 978-953-51-0591-6, InTech, Available from: http://www.intechopen.com/books/metamaterial/design-and-characterization-of-metamaterials-for-optical-and-radio-communications

INTECH
open science | open minds

InTech Europe
University Campus STeP Ri
Slavka Krautzeka 83/A
51000 Rijeka, Croatia
Phone: +385 (51) 770 447
Fax: +385 (51) 686 166
www.intechopen.com

InTech China
Unit 405, Office Block, Hotel Equatorial Shanghai
No.65, Yan An Road (West), Shanghai, 200040, China
中国上海市延安西路65号上海国际贵都大饭店办公楼405单元
Phone: +86-21-62489820
Fax: +86-21-62489821

© 2012 The Author(s). Licensee IntechOpen. This is an open access article distributed under the terms of the Creative Commons Attribution 3.0 License, which permits unrestricted use, distribution, and reproduction in any medium, provided the original work is properly cited.

IntechOpen

IntechOpen